BMC Complementary Medicine and Therapies

RESEARCH

Open Access

Characterization, biological activity, and anticancer effect of green-synthesized gold nanoparticles using *Nasturtium officinale* L.

Ozlem Tonguc Yayintas[1*], Neslihan Demir[2], Fadime Canbolat[3], Tülay Kiliçaslan Ayna[4] and Melek Pehlivan[5]

Abstract

Background Nanostructured materials used have unique properties and many uses in nanotechnology. The most striking of these is using herbal compounds for the green synthesis of nanoparticles. Among the nanoparticle types used for green synthesis, gold nanoparticles (AuNPs) are used for cancer therapy due to their stable structure and non-cytotoxic. Lung cancer is the most common and most dangerous cancer worldwide in terms of survival and prognosis. In this study, *Nasturtium officinale* (L.) extract (NO), which contains biomolecules with antioxidant and anticancer effects, was used to biosynthesize AuNPs, and after their characterization, the effect of the green-synthesized AuNPs against lung cancer was evaluated in vitro.

Methods Ultraviolet–visible (UV–Vis) spectrophotometry, scanning electron microscopy (SEM), transmission electron microscopy (TEM), energy dispersive X-ray spectroscopy (EDS), multiple analysis platform (MAP), and Fourier transform infrared (FT-IR) spectroscopy analyses were performed to characterize the AuNPs prepared from the *N. officinale* plant extract. Moreover, the antioxidant activity, total phenolic and flavonoid contents and DNA interactions were examined. Additionally, A549 lung cancer cells were treated with 2–48 µg/mL *Nasturtium officinale* gold nanoparticles (NOAuNPs) for 24 and 48 h to determine the effects on cell viability. The toxicity of the synthesized NOAuNPs to lung cancer cells was determined by the 3-(4,5-dimethylthiazol-2-il)-2,5-diphenyltetrazolium bromide (MTT) assay, and the anticancer effect of the NOAuNPs was evaluated by apoptosis and cell cycle analyses using flow cytometry.

Results The average size of the NPs was 56.4 nm. The intensities of the Au peaks from EDS analysis indicated that the AuNPs were synthesized successfully. Moreover, the in vitro antioxidant activities of the NO and NOAuNPs were evaluated; these materials gave values of 31.78 ± 1.71% and 31.62 ± 0.46%, respectively, in the 1,1-diphenyl-2-picrylhydrazyl (DPPH) assay at 200 g/mL and values of 25.89 ± 1.90% and 33.81 ± 0.62%, respectively, in the 2,2′-azino-bis(3-ethylbenzothiazoline-6-sulfonic acid) (ABTS) assay. The NO and NOAuNPs gave values of 0.389 ± 0.027 and 0.308 ± 0.005, respectively, in the ferrous ion reducing antioxidant capacity (FRAP) assay and values of 0.078 ± 0.009 and 0.172 ± 0.027, respectively, in the copper ion reducing antioxidant capacity (CUPRAC) assay. When the DNA cleavage activities of NO and the NOAuNPs were evaluated via hydrolysis, both samples cleaved DNA starting at a concentration of 25 g/mL in the cell culture analysis, while the nanoformulation of the NO components gave greater therapeutic and anticancer effects. We determined that the Au nanoparticles were not toxic to A549 cells. Moreover, after treatment with the half-maximal inhibitory concentration (IC_{50}), determined by the MTT assay

*Correspondence:
Ozlem Tonguc Yayintas
oyayintas@comu.edu.tr
Full list of author information is available at the end of the article

with A549 cells, we found that at 24 and 48 h, while the necrosis rates were high in cells treated with NO, the rates of apoptosis were greater in cells treated with NOAuNPs. Notably, for anticancer treatment, activating apoptotic pathways that do not cause inflammation is preferred. We believe that these results will pave the way for the use of NOAuNPs in in vitro studies of other types of cancer.

Conclusion In this study, AuNPs were successfully synthesized from *N. officinale* extract. The biosynthesized AuNPs exhibited toxicity to and apoptotic effects on A549 lung cancer cells. Based on these findings, we suggest that green-synthesized AuNPs are promising new therapeutic agents for lung cancer treatment. However, since this was an in vitro study, further research should be performed in in vivo lung cancer models to support our findings and to explain the mechanism of action at the molecular level.

Keywords *Nasturtium officinale* (L.), Gold nanoparticles, Green synthesis, A549 cell line, Cytotoxic effect

Introduction

Plants have been used for both nutrition and as therapeutic agents to treat health problems since ancient times. In recent years, the WHO reports that over 80% of the world's population gets primary medical care from traditional medications, mostly plants [1, 2]. Plants are frequently used to treat chronic medical conditions such as breast cancer, liver disease, human immunodeficiency virus (HIV) infection, asthma, and rheumatologic disorders [3, 4]. Many epidemiological studies have shown an inverse relationship between Cruciferae plant consumption and the development of cancers such as lung, breast, prostate, stomach, and colon/rectum cancer [5–9]. The Cruciferae (Brassicaceae) family may reduce cancer risk by regulating biotransformation enzymes [10]. The Cruciferae family includes plants such as broccoli, horseradish, cabbage, cauliflower, and watercress. These plants contain high levels of glucosinolate components. Glucosinolates are converted to isothiocyanates (ITCs) nonenzymatically by physical means or enzymatically by myrosinase during food preparation, cooking, and chewing [11]. For example, gluconasturtiin in watercress is hydrolyzed to phenethyl isothiocyanate (PEITC) [12]. Watercress, known by its botanical name *Nasturtium officinale* (L.) is a fast-growing, aquatic, or semiaquatic annual plant whose pharmacological activity has been investigated in cancer studies. Watercress contains high concentrations of glucosinolates; however, glucosinolates are hydrolyzed to ITCs by myrosinase (thioglucoside glucohydrolase; EC 3.2.3.1). Additionally, gluconasturtiin (2-phenyl ethyl glucosinolate) is a member of the glucosinolate class among the aliphatic and indole structures of watercress components [13, 14]. Watercress is also high in carotenoids such as carotene, lutein, and zeaxanthin, in addition to flavonoid compounds, such as quercetin, kaempferol, and isorhamnetin [15]. Watercress is an excellent source of vitamins and antioxidants. It contains vitamins B1, B2, C, and A and folic acid, iodine, iron, protein, calcium, and sulfur compounds, particularly those that contribute to its distinctive odor, which enhances its nutritional value. Watercress is high in antioxidants that protect against cell damage caused by free radicals, which are harmful molecules that cause oxidative stress. Chronic diseases such as diabetes, cancer, and cardiovascular disease have all been linked to oxidative stress. In addition, the anticancer potency of watercress has been intensively studied by various groups and was shown to be due to its high contents of (i) aliphatic, indolyl and aromatic ITCs and (ii) various polyphenolic compounds (e.g., quercetin-3-O-rutinoside, p-coumaric acid and ferulic acid). Notably, Kyriakou et al. [16] reported that watercress is an excellent source of PEITC (273.89 ± 0.88 ng/g dry extract), quercetin (1459.30 ± 12.95 ng/g dry extract) and kaempferol-3-O-rutinosides (257.54 ± 2.31 ng/g dry extract).

The bioactivity of watercress (especially its bioactive component PEITC) largely depends on absorption, metabolism, distribution, and excretion by the human body. Despite various cellular and animal models confirming the benefits watercress has against cancer, the clinical utilization of watercress is still limited due to its low solubility, stability, and bioavailability. To overcome these drawbacks, scientists have recently developed nanodelivery technology, by which nanomaterials have been employed as transport molecules to carry bioactive molecules for therapeutic synergism in cancer treatment. Different types of nanodelivery systems have been developed for this purpose. Metal nanoparticles are one of the main nanodelivery systems used in cancer therapy [17]. The rich bioactive components contained in aquatic plants are often used in metal oxide synthesis due to their ability to oxidize metal particles. Plant extracts can reduce metal nanoparticles after they interact with metal ions [18]. Gold nanoparticles (AuNPs) are biomaterials that are easily synthesized with sizes and shapes that can be adjusted and surface functionalities that can be changed by ligand binding. AuNPs are inert, biocompatible, and nontoxic [19]. By modifying AuNPs, they can selectively target certain cells and even to organelles within these cells [20]. These properties have allowed AuNPs to be

used as biosensors, drug delivery carriers, gene therapy agents and theranostic agents. AuNPs, as some of the most commonly used particles in nanotechnology, have been used in various medical treatments for centuries without harmful effects [21, 22]. The in vitro biological activity of AuNPs obtained using the aqueous extract of *Rosa damascena* were used toward the development of plant-mediated chemistry. AuNPs are ultrasmall, stable, and biocompatible with unique physicochemical properties, such as a large surface area-to-mass ratio and high surface reactivity [23]. AuNPs can be considered drug delivery systems due to their unique physicochemical properties, biocompatibility, surface plasmon resonance (SPR), optical properties, tunability and easy surface modification and can be prepared in a wide range of sizes (1–100 nm). AuNPs are commonly used as drug delivery systems after surface modification with cationic polymers or reactive functional groups (e.g., amine, thiol, or carboxyl groups). AuNPs are efficient nanocarriers for various active substances, such as peptides, proteins, plasmid DNAs (pDNAs), small interfering RNAs (siRNAs) and chemotherapeutic agents [23–25]. Green synthesis methods have also been developed as nanotechnology advances. AuNPs can be synthesized in a green manner using algae and plant extracts [26]. AuNPs have been generated using a variety of plant extracts, including those from *Aloe vera*, *Trigonella foenum-graecum*, *Citrus sinensis* peels, *Cinnamomum zeylanicum*, *Medicago sativa*, Tamarind leaves, and *Rosa rugosa* [27–33]. Mobaraki et al. [34] used the *N. officinale* leaf extract as a reducing and stabilizing agent, resulting in AuNPs with an average size of 64 nm and dose-dependent 1,1-diphenyl-2-picrylhydrazyl (DPPH) scavenging ability. AuNPs given to male rats prevented testicular damage and may provide a rational and potential source for a new chemotherapy drug conjugation system.

The aim of our study was to synthesize *N. officinale* gold nanoparticles (NOAuNPs) with green synthesis method and assess their cytotoxic, anticancer, and apoptotic effects on a lung cancer cell line (A549). For this purposes, the NOAuNPs were characterized by ultraviolet–visible (UV–Vis) spectrophotometry, scanning electron microscopy (SEM), transmission electron microscopy (TEM), energy dispersive X-ray spectroscopy (EDS), multiple analysis platform (MAP), and Fourier transform infrared (FT-IR) spectroscopy analyses. Moreover, the antioxidant activity, total phenol and flavonoid contents, and DNA interactions were investigated. A real-time cell assay and 3-(4,5-dimethylthiazol-2-yl)-2,5-diphenyl tetrazolium bromide (MTT) assays were used to assess the toxic effects of the NOAuNPs to cancer cells, and apoptosis and cell cycle analyses were used to assess their anticancer effects.

Materials and methods

Standards and reagents

1,1-Diphenyl-2-picrylhydrazyl (DPPH), 2,2'-azino-bis(3-ethylbenzothiazoline-6-sulfonic acid) (ABTS), 2,4,6-tris(2-pyridyl)-S-triazine (TPTZ), neocuproine, and tetrachloroauric acid ($HAuCl_4.3H_2O$) were purchased from Sigma Aldrich, USA. Folin–Ciocalteu phenol reagent, gallic acid, hydrochloric acid (HCl), ferric chloride hexahydrate ($FeCl_3.6H_2O$), and ammonium acetate were purchased from Merck, Germany. Quercetin was purchased from Carl ROTH, Germany. Sodium acetate was purchased from Isolab Chemicals (Germany). $CuCl_2.2H_2O$ was purchased from Carlo Erba, Italy. Dulbecco's modified Eagle's medium (DMEM), 100 U/ml penicillin and 100 g/ml streptomycin were obtained from Gibco; L-glutamine was obtained from Sigma–Aldrich, USA; the 3-(4,5-dimethylthiazol-2-yl)-2,5-diphenyl tetrazolium bromide (MTT) assay kit and Annexin V-FITC/7AAD were obtained from Elabscience, Texas, USA; and a cell cycle kit was obtained from Invitrogen, Carlsbad, CA, USA.

Plant material and preparation of the *Nasturtium officinale* extract

The plant leaf was collected near Gökköy, Umurbey district, Canakkale province, Turkey, from a fruit garden on both sides of the Umurbey stream. The collected species were identified by Prof. Dr. Özlem YAYINTAŞ, a faculty member of Çanakkale Onsekiz Mart University Faculty of Medicine, Department of Medical Biology and personal herbarium number T 1 (T: Tonguc). The *N. officinale* plants were washed twice with distilled water and allowed to dry. Ten grams of the plant sample was subjected to extraction with 100 mL of methanol at 70 °C for 1 h and then filtered through Whatman filter paper (No. 1).

Synthesis of gold nanoparticles (AuNPs) using *Nasturtium officinale* (L.) extract

At room temperature, 90 mL of 1 mM tetrachloroauric acid ($HAuCl_4.3H_2O$) and 10 mL of the methanolic plant extract were mixed. After discoloration, the solution was centrifuged for 30 min at 7500 rpm. Washing with ultrapure water was performed twice at 7500 rpm. The pellet was dried in an oven at 60 °C.

Characterization of green-synthesized gold nanoparticles (AuNPs)

The AuNPs synthesized via the green method were characterized using SEM, TEM, EDS, MAP, FT-IR and UV–Vis to determine their physical characteristics [35]. The UV–visible (UV–Vis) spectrum of the NPs was acquired by employing a T80 + UV/VIS Spectrometer (PG Instruments Ltd., U.K.) in the range of 200–500 nm. The functional groups found in the extract and synthesized AuNPs were identified

by scanning on a Fourier transform infrared spectrophotometer (Perkin Elmer BX II FT spectrometer, Massachusetts, U.S.) in the range of 400–4000 cm^{-1}. Morphological examination of the synthesized AuNPs was carried out using SEM (JEOL JSM5600, Japan), and quantitative elemental analysis of the synthesized AuNPs was performed via EDS and MAP.

Determination of the total flavonoid content

The total flavonoid content of the extract was determined according to the method described by Matejić et al. [36]. Quercetin was used as the standard in this study. The absorbance value of the mixture kept at room temperature for 40 min was measured at 415 nm with a spectrophotometer. The total amount of flavonoids contained in the extract is presented as milligrams of quercetin equivalents (QE) per gram of extract (mg QE/g).

Determination of the total phenolic content

The total phenolic content of the extract was determined using *Folin–Ciocalteu* reagent, as described by Slinkard and Singleton [37]. The standard phenolic compound was gallic acid (GA). The absorbance values of the prepared samples were measured with a spectrophotometer at 760 nm and recorded. Each experiment was repeated three times, and the results were averaged. The total phenolic content of the plant is presented as milligrams of gallic acid equivalents per gram of extract (mg GAE/g).

Antioxidant activity

DPPH radical scavenging activity

The free radical scavenging activities of the synthesized NOAuNPs and NO were determined by the 1,1-diphenyl-2-picrylhydrazyl (DPPH) method [38]. Different concentrations of the NO and NOAuNP samples were added to spectrophotometry cuvettes, mixed with DPPH solution and incubated in the dark for 30 min at room temperature, after which their absorbance values were measured at 517 nm in the dark 3 times. Butylated hydroxytoluene (BHT) was used as the standard. The measured absorbance values were substituted into Eq. 1 below to calculate percent inhibition:

$$\% \text{ Inhibition} = [(\text{Abs}_{\text{control}} - \text{Abs}_{\text{sample}})/\text{Abs}_{\text{control}}] \times 100 \quad (1)$$

where $\text{Abs}_{\text{sample}}$ is the absorbance of the sample and $\text{Abs}_{\text{control}}$ is the absorbance of the blank solution.

ABTS method

The radical scavenging capacities of the NOAuNPs and NO were determined using the ABTS [2,2'-azino-bis(3-ethylbenzothiazoline-6-sulfonic acid)] cation radical scavenging method [39]. ABTS reagent (7 mM ABTS and 2.45 mM potassium persulfate) was applied to the NOAuNP and NO samples prepared at various concentrations. Then, the absorbance of the blue/green ABTS reagent at 734 nm was adjusted to 0.7 using an ethanol–water (60%-40%) mixture. The ABTS reagent was incubated with the samples for 6 min at room temperature. The absorbance values of the samples were then measured at 734 nm against the blank. The formula in Eq. 1 was used to calculate the % ABTS radical scavenging inhibition from the measured values.

Ferrous ion reducing antioxidant capacity (FRAP) method

The FRAP test was performed according to the method of Benzie and Strain [40]. The samples were incubated in the dark for 30 min after the FRAP reagent (0.3 M sodium acetate, 10 mM 2,4,6-tris(2-pyridyl)-S-triazine (TPTZ), and 20 mM $FeCl_3$; 10:1:1) was added. After incubation in the dark, the absorbance values of the samples were measured at 593 nm. BHT was used as a positive control, and each experiment was repeated three times.

Copper ion reducing antioxidant capacity (CUPRAC) method

The antioxidant capacities of the synthesized nanoparticles and extract were determined by the copper ion reducing antioxidant capacity (CUPRAC) method. First, 10 mM $CuCl_2$ (250 µL), 7.5 mM neocuproine (250 µL) and 1 M ammonium acetate (250 µL) were added to the NO and NOAuNP samples, which ranged in concentration from 6.25–200 µg/mL. After the total volume of each sample was adjusted to 1000 µL, and the absorbance values of the solutions were measured at 450 nm [41].

Nanoparticle (NP) interactions with DNA

For DNA fragmentation studies, pBR322 plasmid DNA (90% supercoiled) was used. When the original supercoiled form (Form I) of plasmid DNA was damaged, it opened to generate a circular form (Form II), after which a linear form (Form III) can also be identified due to further breakage. During gel electrophoresis, Form I moved the fastest, Form II moved the slowest, with Form III appearing between Form I and Form II. To examine hydrolytic activity, plasmid pBR322 DNA was treated with the samples in Tris–HCl buffer (10 mm, pH 7.4), and to investigate oxidative activity, the inducing agent hydrogen peroxide (H_2O_2) was added to the DNA, buffer, and sample mixture. The prepared samples were incubated in an incubator at 37 °C for 3 h before adding 6×loading dye and subjection to gel electrophoresis for 90 min at 60 V in a 0.8% agarose gel with 1×TAE buffer (40 mM Tris-20 mM acetic acid, 1 mM EDTA, pH 8.2).

The bands were then photographed under UV light using a gel imaging system (DNR, Bio-Imaging system).

In vitro cytotoxicity and anticancer effect

A549 cell culture

The lung cancer cell line A549 (ATCC CRM-CCL-185™) was purchased commercially and stored in a liquid nitrogen tank for long-term use. A549 cells were cultured in Dulbecco's modified Eagle's medium (DMEM) (Gibco) supplemented with 10% heat-inactivated fetal bovine serum (FBS) (Serox), 100 U/ml penicillin, 100 g/ml streptomycin (Gibco), and 2 mM L-glutamine (Sigma–Aldrich). The cells were incubated in a 5% CO_2 atmosphere at 37 °C [42].

Preparation of materials for in vitro cytotoxicity assessments

N. officinale extract, AuNPs and NOAuNPs were weighed on a precision balance and dissolved in DMSO. The samples were kept in a sonicator in the dark for 10 min, and after ensuring complete dissolution, the dose needed for the study was calculated.

Cell counting via the trypan blue method

Trypan blue was used to distinguish between live and dead cells and to determine how many live cells should be seeded for further research. Trypan blue was mixed with the cell suspension in an Eppendorf tube at a 1:1 ratio, and 10 µL of the mixed sample was added dropwise to a Neubauer slide. The cells were counted under a microscope after being covered with a coverslip. The formula for calculating the cell number was the mean of counted squares × DF (dilution factor) × 10^4.

3-(4,5-Dimethylthiazol-2-yl)-2,5-diphenyl tetrazolium bromide (MTT) cell proliferation assay

An MTT assay kit (Elabscience) was used to investigate cell viability. MTT is 3-(4,5-dimethylthiazol-2-yl)-2,5-diphenyl tetrazolium bromide, which is reduced in the mitochondria by certain dehydrogenases to form the dark purple crystalline product formazan.

A total of 5×10^3 cells were seeded in each well of a 96-well plate in a volume of 100 µL. The cells were allowed to attach for 24 h. After 24 h, the media in the wells was removed and discarded. NO, AuNPs and NOAuNPs were tested at concentrations of 2, 4, 8, 16, 24, and 48 µg/mL. The half-maximal inhibitory concentration (IC_{50}) was determined after 24 and 48 h [42].

Since a 5× reagent concentration was used in the MTT assay, here, the reagent was diluted to 1× in MTT dilution buffer. To do so, 100 µL of 5× MTT was added to 400 µL of MTT dilution buffer. Then, 50 µL of 1× MTT solution was added to each well, and the plates were incubated for 4 h. At the end of the incubation, the supernatant was removed from each well and discarded. Then, 100 µL of DMSO was added to each well to dissolve the formazan, and the plate was shaken in the reader for 10 min. At the end of the incubation, the absorbance at 570 nm was measured with an ELISA reader (BioTek Instruments). The cell viability of the experimental group was compared to that of the control group by assuming 100% cell viability in the control group [42]. The formula in Eq. 2 was used for calculation:

$$\text{Cell viability}(\%) = \frac{\text{Absorbance of the experimental well}}{\text{Average absorbance of the control well}} \times 100 \quad (2)$$

Determination of the in vitro anticancer effects

Apoptosis analysis by flow cytometry

A total of 2.5×10^5 cells were cultured in each well of a 6-well plate to determine anticancer activity. The IC_{50} values of NO and NOAuNP were calculated, and then NO and the NOAuNPs were added to the appropriate wells for 24 and 48 h of incubation. Furthermore, cells were left untreated in the control group (only the medium was refreshed). A cell scraper was used to collect cells from the wells, which were then washed twice with cold PBS and subjected to Annexin V-FITC/7AAD (Elabscience) double staining according to the manufacturer's instructions. Apoptosis was analyzed using a Beckman DxFLEX flow cytometer with CytExpert Software (Beckman Coulter Life Sciences) [43].

Cell cycle analysis by flow cytometry

Cell cycle analysis was carried out according to the instructions of a commercially purchased kit (Invitrogen). Powdered propidium iodide was diluted to 1 mg/mL (1.5 mM) with deionized water to generate a stock solution, which was diluted 1:500 with staining buffer (100 mM Tris, pH 7.4, 150 mM NaCl, 1 mM $CaCl_2$, 0.5 mM $MgCl_2$, 0.1% Nonidet P-40) to generate the dilution solution.

A549 cells were seeded in 6-well plates at a density of 2.5×10^5 cells per well. The medium was removed from the wells after 24 h. The wells were given the IC_{50} dose of the appropriate material for 24 or 48 h of incubation. The cells from the untreated control and treatment wells (NO and NOAuNPs) were then collected in flow cytometry tubes using a cell scraper and washed with 1 mL of PBS. In a cold environment, 4 mL of 96–100% ethanol was added, and each mixture was incubated at -20 °C for 15 min. Then, the supernatant was removed by centrifugation. After 15 min of standing at room temperature, 5 mL of PBS was added to each cell pellet. The tubes were centrifuged at the end of the incubation period to remove

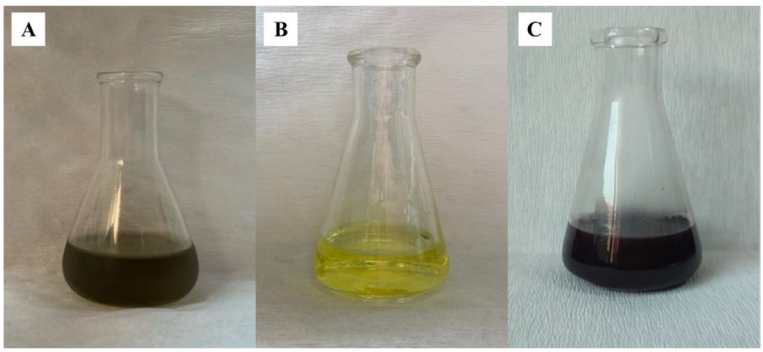

Fig. 1 Color change transformation during extract synthesis. **A** NO, **B** $HAuCl_4.3H_2O$, and **C** NOAuNPs

the supernatant. Each tube then received 1 mL of PI staining buffer and was gently vortexed, followed by analyses by DxFLEX flow cytometry and CytExpert software.

In silico analysis

Drug likeness and absorption, distribution, metabolism, excretion, and toxicity (ADMET) analysis

According to various studies, PEITC can effectively target a wide spectrum of cancer-related proteins. PEITC was included in our ADMET and docking analyses. PEITC was subjected to drug likeness tests by checking for Lipinski's rule of five (Ro5) violations [44–47]. For ADMET predictions, the SwissADME (http://www.swissadme.ch (accessed on 15 January 2023) [35] and pkCSM (https://biosig.lab.uq.edu.au/pkcsm/(accessed on 15 January 2023) servers were used [48, 49]. First, the molecular simplified molecular input line entry system (SMILES) structure of PEITC was downloaded from PubChem (http://pubchem.ncbi.nlm.nih.gov/) (accessed on 15 January 2023). The downloaded SMILES structure was then uploaded to the servers. The physicochemical and ADMET properties of PEITC were evaluated using the standard program parameters.

Docking analysis

Our investigation evaluated the effects of PEITC from in *N. officinale* on cytochrome P450 enzymes (CYP450s) and tubulin in terms of cancer mechanisms. Following protein structure selection guidelines [50], protein structures were downloaded from the Protein Data Bank (PDB) (Table 4) to determine the impact of the pharmacological profile of the cocrystallized ligand on docking performance. To identify the best docking protocol for PEITC predictions, we used the dataset accompanying the access software program UCSF Chimera (https://www.cgl.ucsf.edu/chimera/ (accessed on 15 January 2023)) on the PDB structures. Visualization of the results was performed using the Discovery Studio program (https://discover.3ds.com/discovery-studio-visualizer-download (accessed on 15 January 2023)).

Statistical analysis

GraphPad Prism 21 was used to analyze all the cell viability and cell cycle data. Analyses were performed three times, and the means and standard deviations of the results were calculated. One-way ANOVA was used to determine the significance of the differences between groups. The significance level was set at $p < 0.05$.

Results

Characterization of the *N. officinale* gold nanoparticles (NOAuNPs)

Morphological observations

The formation of gold nanoparticles was evident when the color of the extract changed from green to violet–purple (Fig. 1).

Scanning electron microscopy (sem) and transmission electron microscopy (TEM) analyses

According to the SEM images, the average size of the NPs was 56.4 nm (Fig. 2A). Because some small particles overlapped, large NPs can be observed due to clustering. TEM analysis confirmed the presence of spherical nanoparticles (Fig. 2B).

Energy dispersive X-ray spectroscopy (EDS) and multiple analysis platform (MAP) analysis

The intensity of the EDS Au peaks indicates that the synthesis of the Au nanoparticles was successful (Fig. 3A). Elements such as C and O in the green-synthesized NOAuNPs using *N. officinale* may be derived from the plant or the water used during synthesis. MAP analysis of the nanoparticles revealed that Au accounted for 71.84% of the material weight (Table 1). Figure 3B shows the density of Au.

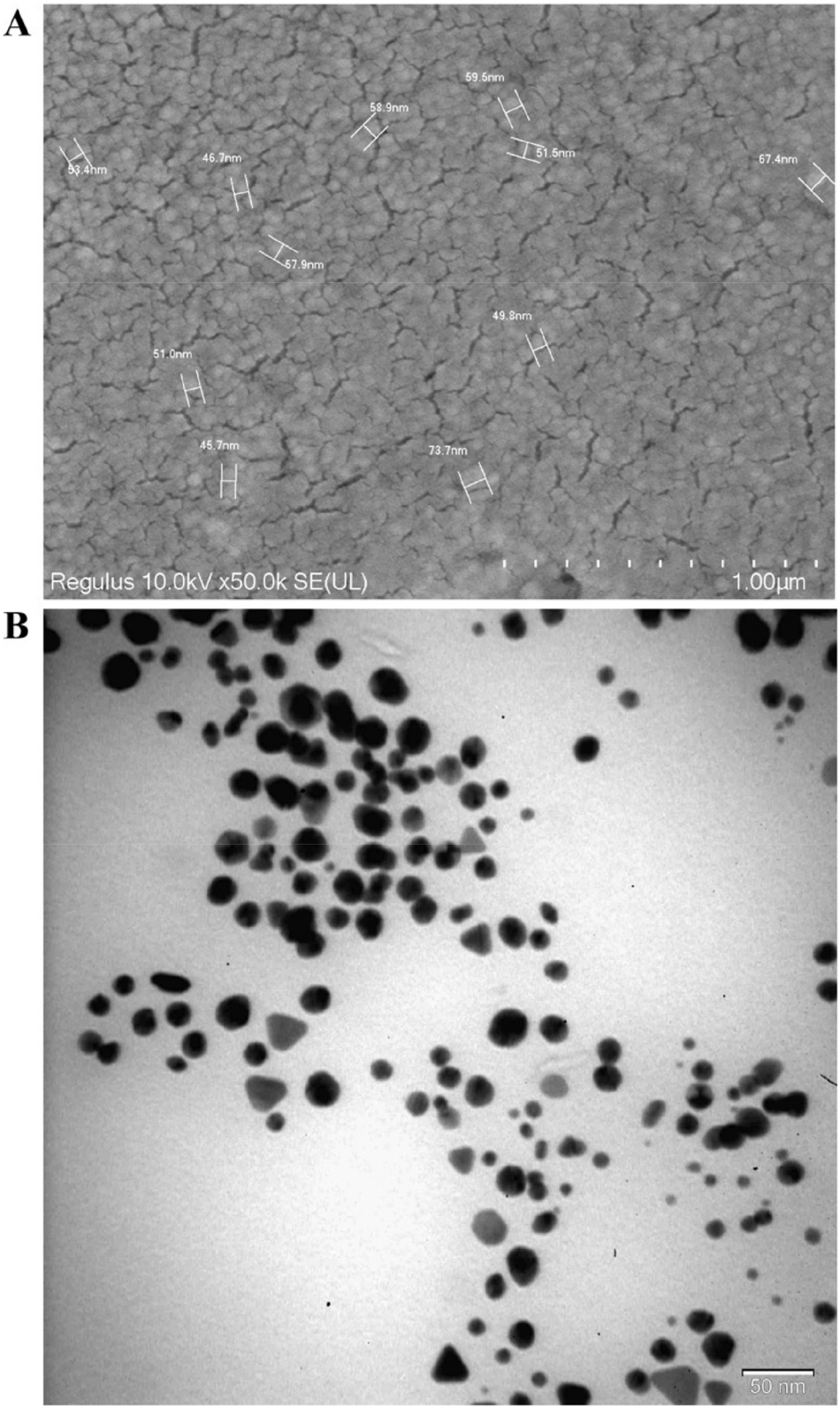

Fig. 2 Morphological observations. **A** SEM image of the NOAuNPs. **B** TEM image of the NOAuNPs

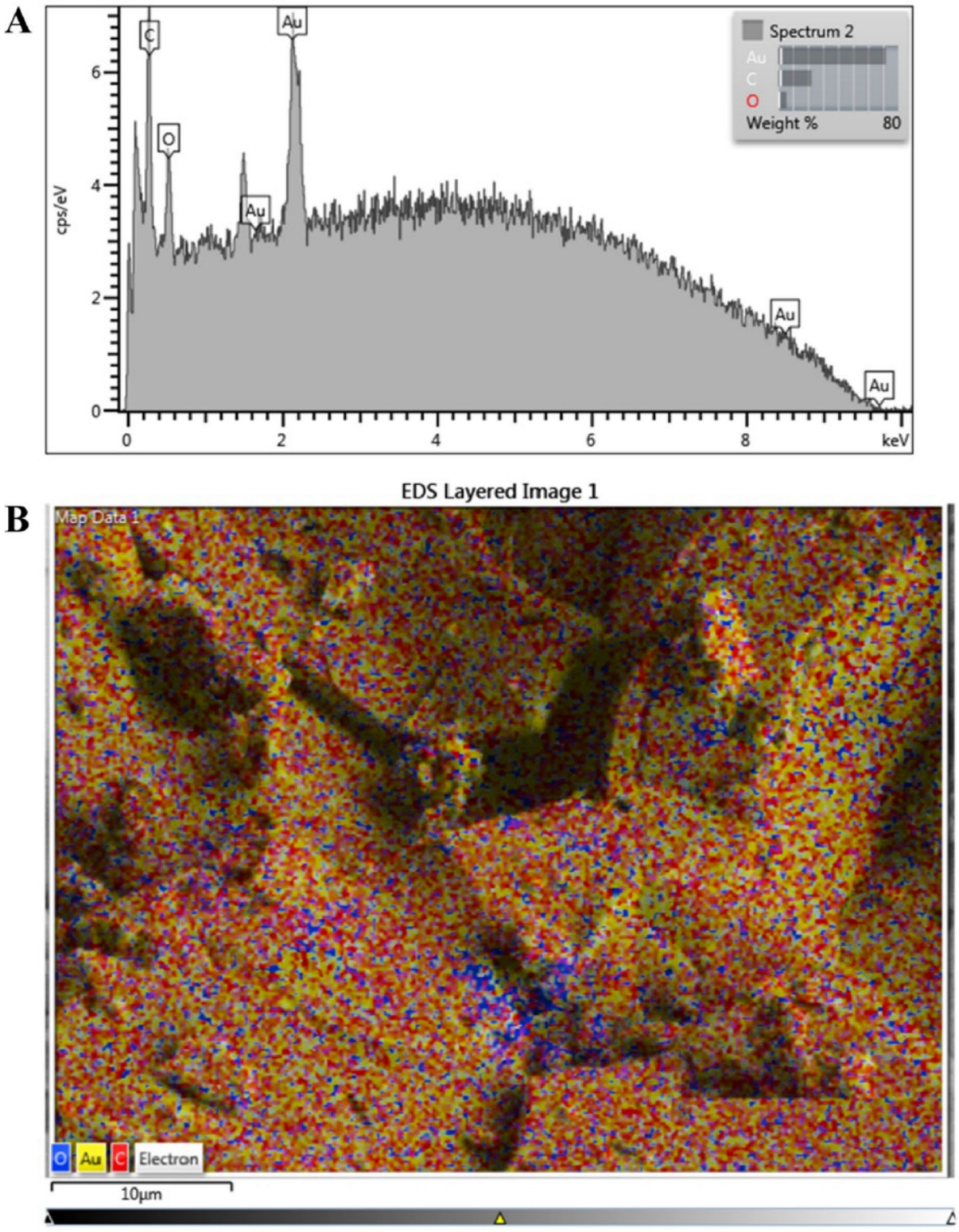

Fig. 3 EDS and MAP analyses of the NOAuNPs. **A** EDS and **B** MAP

Table 1 EDS analysis of the NOAuNPs

Element	Weight (%)	Weight (%) Sigma
C	22.37	1.98
O	5.79	0.86
Au	71.84	2.27
Total	100.00	

Fourier transform infrared (FT-IR) spectroscopy and UV–visible (UV–Vis) spectroscopy

N. officinale contains alkaloids, flavonoids, saponins, terpenoids/steroids, proteins, volatile and essential oils, glycosides, tannins, folic acid, vitamins, and various elements according to chemical analysis. According to the FTIR spectrum of *N. officinale*, the peaks observed at 3853, 3744, 3444, and 3262 cm^{-1} were attributed to the vibrations of the OH, NH_2, NH and COOH groups in the alkaloids, tannins, folic acid, and vitamins in the plant. The vibrations observed at 2960 and 2922 cm^{-1} in the spectrum were assigned to the methyl groups of alkaloids. The strong vibration at 1739 cm^{-1} was due to the ketone groups (C = O) in the flavonoids, saponins, terpenoids/steroids, and glycosides. The vibration at 1698 cm^{-1} was attributed to the tannins, folic acid and vitamins containing acidic COOH groups. The strong vibration observed at 1646 cm^{-1} in the FT-IR spectrum were assigned to the C = N groups in glycosides. In all the samples, the peak at 1556 cm^{-1} was attributed to C = C vibrations, and the peak at 1458 cm^{-1} was attributed to C–N vibrations. C-O and C–O–C vibrations were observed at 1397, 1173, 1113, and 1047 cm^{-1} (Fig. 4A).

According to the FTIR spectrum of the NOAuNPs, the peaks at 3853, 3262, 2922, and 1740 cm^{-1} remained unchanged and very similar, but the peak at 1698 cm^{-1} was not observed in the spectrum of *N. officinale*. This indicates that the COOH groups in NO reduced the gold to form NOAuNPs, while the COOH groups were oxidized to CO_2. The C = N vibrations from glycosides were observed at 1640 cm^{-1} in the spectrum. This demonstrates that the C = N bonds remain stable throughout the reduction event. C = C, C-N, C-O, and C–O–C vibrations were detected in the FTIR spectrum of the AuNPs at 1560, 1517, 1458, and 1398 cm^{-1} and at 1165, 1112, and 1051 cm^{-1}, respectively (Fig. 4A). As a result, it can be concluded from the FTIR analysis that the NOAuNPs had formed, the gold was reduced, and the COOH groups in NO were oxidized. A maximum absorbance peak at 382 nm (value of 1.646) was obtained from UV–Vis analysis of the synthesized NOAuNPs (Fig. 4B).

Total flavonoid/phenolic contents and analysis of antioxidant activity

The total flavonoid content of the methanol extract was determined to be 6.81 mg QE/g, and the total phenolic content was determined to be 4.32 mg GAE/g.

The antioxidant activities of the NOAuNPs and NO were investigated by determining their 1,1-diphenyl-2-picrylhydrazyl (DPPH), radical scavenging activity, 2,2'-azinobis(3-ethylbenzothiazoline-6-sulfonic acid) (ABTS), cation radical scavenging activity, ferrous ion reducing antioxidant capacity (FRAP), and copper ion reducing antioxidant capacity (CUPRAC).

The results revealed that compared with the extract, the NOAuNPs had greater antioxidant activity. When the DPPH free radical scavenging activities of the extract and NOAuNPs were evaluated, the highest inhibition values were 31.78 ± 1.71% and 31.62 ± 0.46%, respectively, at 200 g/mL (Fig. 5A). When the ABTS cation radical scavenging activities of the extract and NOAuNPs were tested, the % inhibition values at the highest concentration (200 g/mL) were 25.89 ± 1.90 and 33.81 ± 0.62, respectively (Fig. 5B).

In the FRAP activity assays, the highest absorbance values for the extract and NOAuNP were 0.389 ± 0.027 and 0.308 ± 0.005, respectively, at a concentration of 200 µg/mL (Fig. 6A). In the CUPRAC assay, the highest absorbance values for the extract and NOAuNPs were 0.078 ± 0.009 and 0.172 ± 0.027, respectively (Fig. 6B).

Interactions of NO and the NOAuNPs with DNA

When the DNA cleavage activity of NO and the NOAuNPs was evaluated by hydrolysis, it was discovered that both samples cleaved DNA starting at a concentration of 25 µg/mL. When the samples were tested under oxidative conditions, both were found to cleave DNA in the presence of H_2O_2 (Fig. 7).

Cell viability test

A549 cells were treated with the NO, AuNP and the NOAuNPs at the indicated doses for 24 h. At concentrations from 2 µg/mL to 48 µg/mL, AuNP had little effect on cell viability; even at the highest dose of 48 µg/mL, approximately 85% cell viability was observed after 24 h. A549 cells treated with NO extract alone showed a dose-dependent decrease in cell viability, with 74% viability after treatment with 48 µg/mL for 24 h, while the A549 cells treated with the NOAuNPs showed a decrease in cell viability (below 50%) after 24 h at the highest dose of 48 µg/mL (Fig. 8A).

A549 cells were treated with the same doses of the NOAuNPs, NO and Au, and the cell viability after 48 h was evaluated. The NOAuNPs decreased the viability

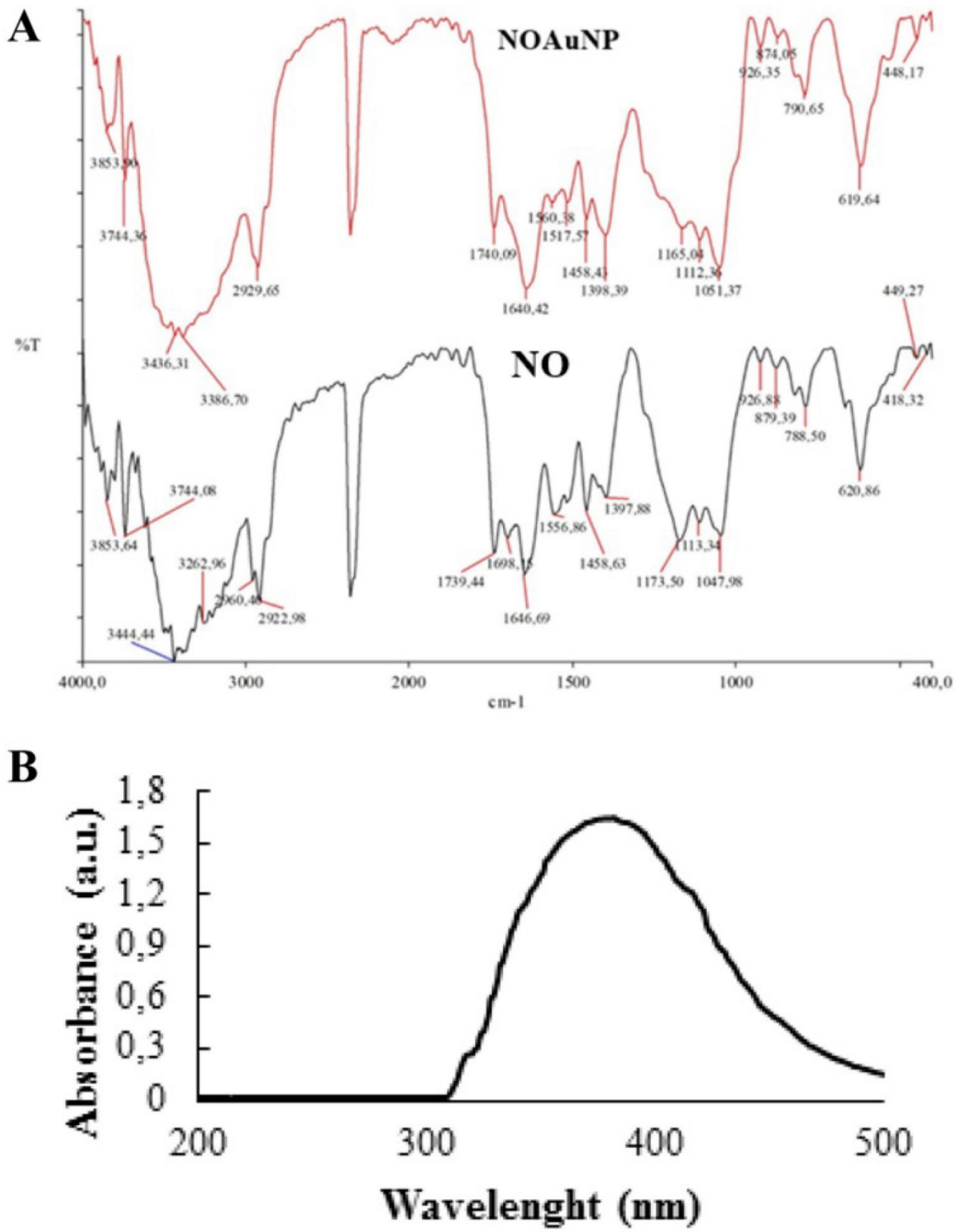

Fig. 4 Spectroscopic analyses. **A** FT-IR spectra of NO and the NOAuNPs. **B** UV–Vis spectrum of the NOAuNPs

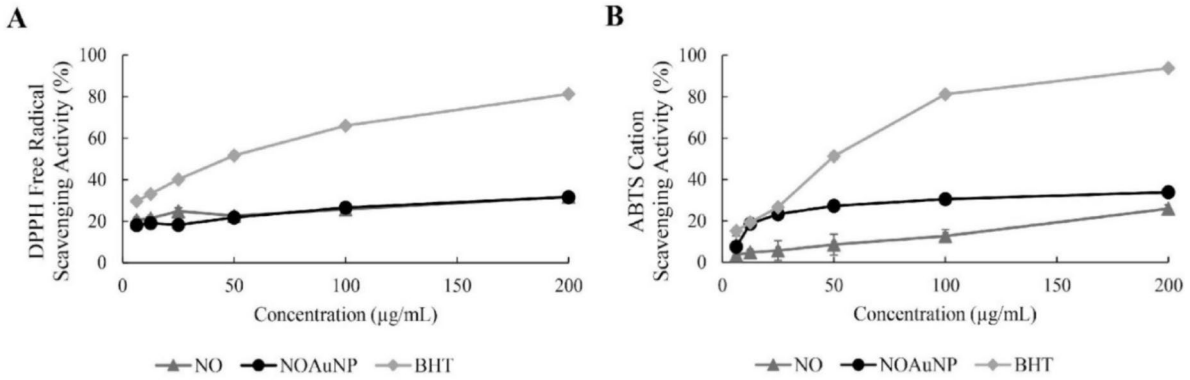

Fig. 5 DPPH and ABTS analyses. Graphs of the **A** 1,1-diphenyl-2-picrylhydrazyl (DPPH) radical scavenging activity and **B** ABTS cation radical scavenging activity

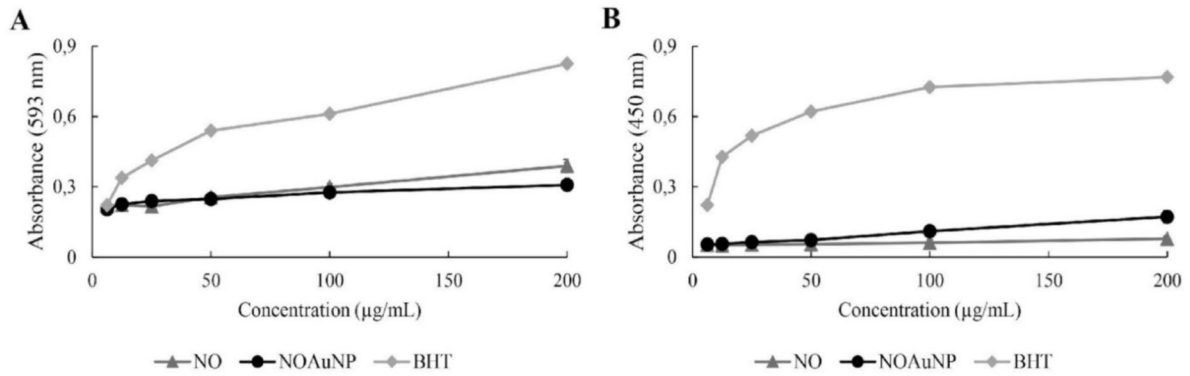

Fig. 6 FRAP and CUPRAC analyses. Graphs of the **A** ferrous ion reducing antioxidant capacity (FRAP) activity and **B** copper ion reducing antioxidant capacity (CUPRAC) activity

of A549 cells in a dose-dependent manner, and 43% of the cells were viable at the highest dose of 48 µg/mL. At the highest dose of NO alone, A549 cell viability was 76%. When the effect of AuNP on cell viability was assessed after 48 h, it was discovered that there was an extremely low cytotoxicity, and cell viability was approximately 104%, even at the highest dose (Fig. 8B).

Our results at 24 and 48 h showed that the Au nanoparticles applied at various doses were not toxic to A549 cells, and compared with the results after the NO extract was applied directly to the cells, NOAuNPs reduced the viability of the A549 cells. This demonstrated that when the NO was combined with Au nanoparticles, it killed nearly half of the cells in a dose-dependent manner. The IC_{50} values of the NOAuNPs were determined to be 39.84 µg/mL after 24 h and 25.05 µg/mL after 48 h using the program GraphPad (Fig. 9).

Anticancer effects

Apoptosis analysis by flow cytometry

Phosphatidylserine (PS) on the cytoplasmic surface of the cell membrane in living cells translocates to the extracytoplasmic surface of cells undergoing apoptosis. FITC-labeled Annexin V binds to PS on the outer membrane to reveal apoptotic cells. 7-AAD binds to G-C-rich regions of DNA via intercalation. After disruption of the cell membrane and integrity loss, 7-AAD enters late apoptotic and necrotic cells, respectively, and stains their DNA. Cells in various stages of apoptosis and necrotic cells are distinguished when 7-AAD is used in conjunction with Annexin V.

Annexin V-FITC/7-AAD staining was applied to untreated (control) A549 cells and A549 cells treated with NOAuNPs and NO. The results were determined by counting 10.000 cells via flow cytometry. The apoptosis inhibition effects after treatment with the IC_{50} dose were

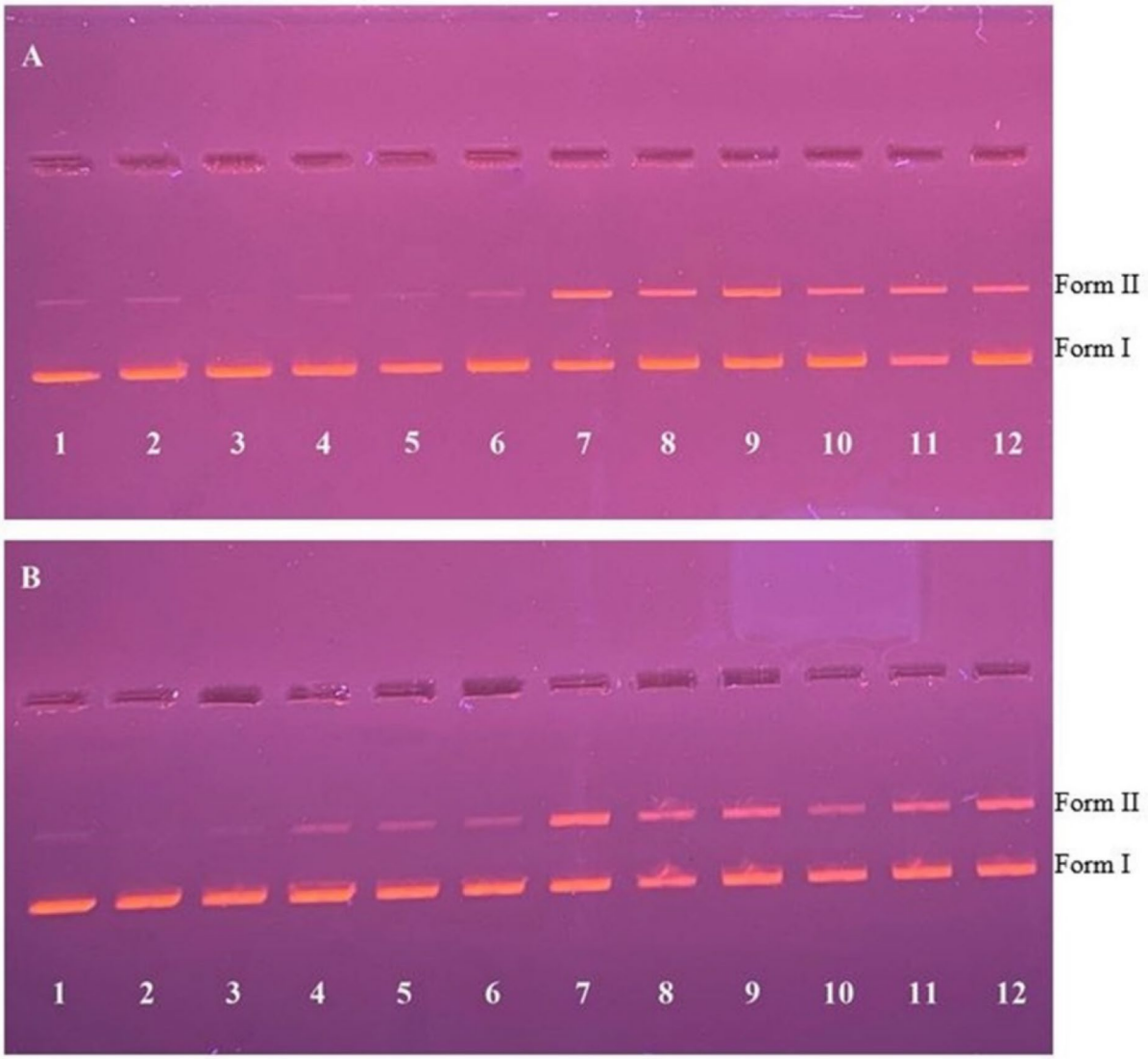

Fig. 7 DNA cleavage activity of **A** NO and **B** NOAuNPs: 1–6 hydrolytic DNA cleavage activity and 7–12 oxidative DNA cleavage activity. 1. pBR322 DNA, 2. DNA + 6.25 µg/mL, 3. DNA + 12.5 µg/mL, 4. DNA + 25 µg/mL, 5. DNA + 50 µg/mL, 6. DNA + 100 µg/mL. 7. DNA + H_2O_2, 8. DNA + 6.25 µg/mL + H_2O_2, 9. DNA + 12.5 µg/mL + H_2O_2, 10. DNA + 25 µg/mL + H_2O_2, 11. DNA + 50 µg/mL + H_2O_2, 12. DNA + 100 µg/mL + H_2O_2

analyzed by flow cytometry. The Annexin V-FITC/7-AAD staining results of the cells after 24 and 48 h are shown in Fig. 10A and B, respectively.

Figure 10A shows the results after treatment with the IC_{50} doses and the results from the untreated control group after 24 h. In the first panel, FS/SS dot plot analysis of the A549 cells in the control group is shown in terms of size and granularity. The cells within gate P1 are A549 cells. The percentages of early apoptotic, late apoptotic, and necrotic cells in the P1 gate are shown in the second panel. These cells were not exposed to any reagents, and the viability rate was 99.81% (lower left, LL). In this group, 0.19% of the cells appeared to have undergone necrosis (upper left, UL). The third panel shows the percentages of early apoptotic (lower right, LR), late apoptotic (upper right, UR) and necrotic A549 cells treated with NOAuNPs. In this group, the P1 gate covering the A549 cells was drawn in the FS/SS dot plot (not shown here), and the cells covered by the P1 gate were evaluated in the third panel. In contrast, 42.92% of the cells treated with the NOAuNPs were viable, 2.54% had undergone early apoptosis, 28.43% had undergone late apoptosis, and 26.12% had undergone necrosis. The apoptotic results of the cells treated with NO are shown in the fourth panel. The FS/SS analysis of the A549 cells treated with the NO extract is not shown in Fig. 10A. However,

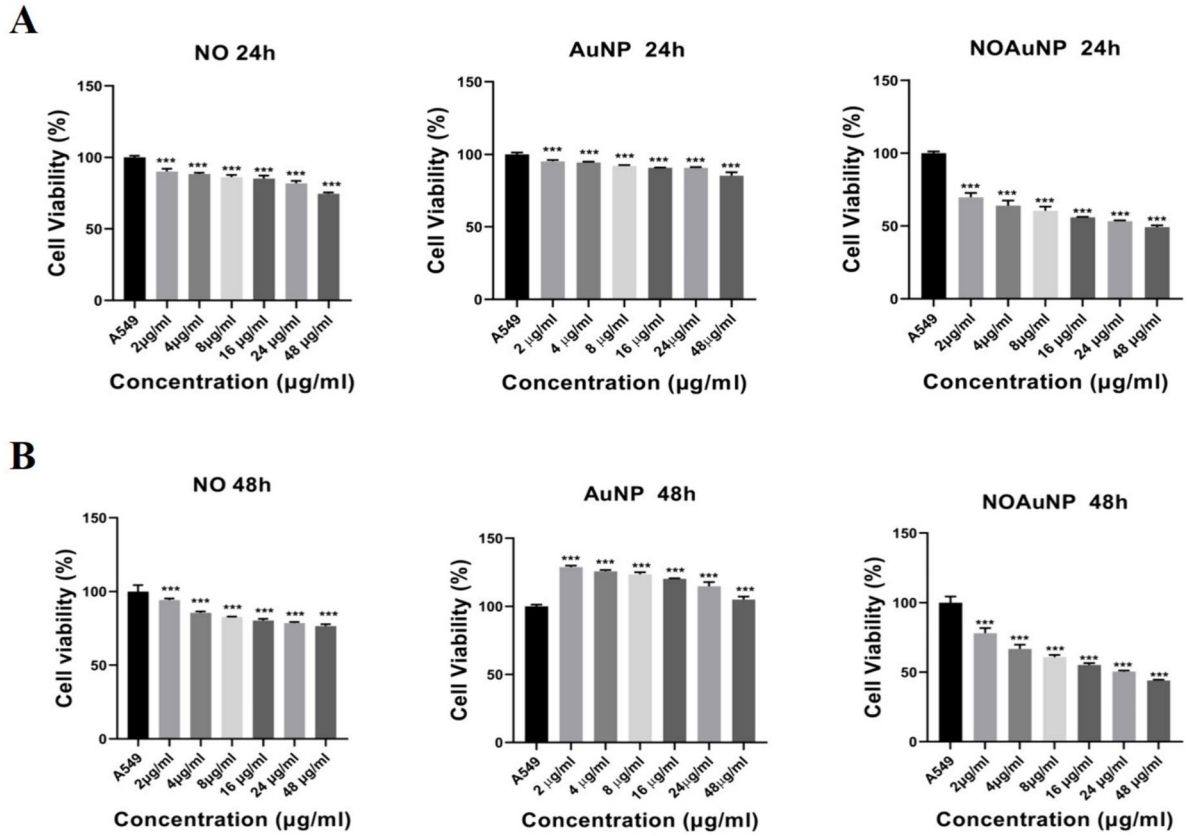

Fig. 8 Viability of A549 cells treated with NO, AuNP and NOAuNPs for 24 (**A**) and 48 (**B**) hours

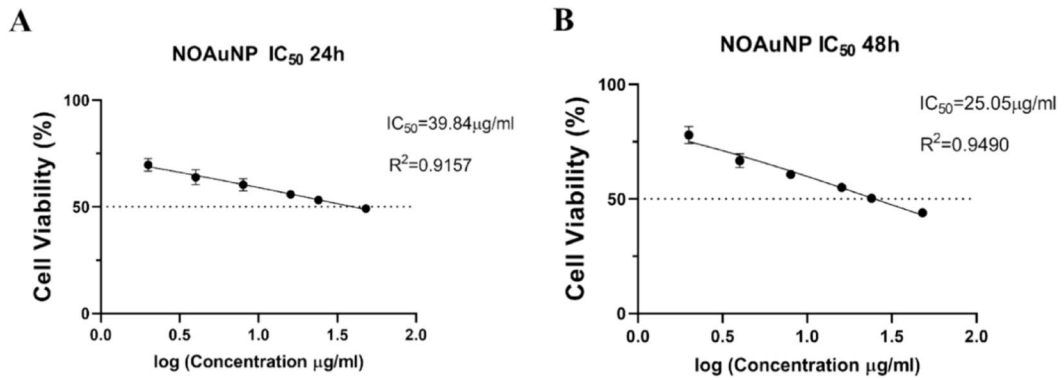

Fig. 9 IC_{50} values of the NOAuNPs after 24 (**A**) and 48 (**B**) hours

21.82% of the cells treated with NO were viable, 1.60% had undergone early apoptosis, 27.52% had undergone late apoptosis, and 49.07% had undergone necrosis.

Figure 10B shows the results of the cells treated at the dose of 48 µg/ml and the untreated control cells after 48 h. The apoptotic control cells in gate P1 in the first panel are shown in the second panel, with a viability rate of 99.81% (LL). The results of FS-SS analysis after treatment with the NOAuNPs and NO for 48 h are not shown in Fig. 10B. In contrast, 42.06% of the cells treated with the NOAuNPs were viable, 2.48% underwent early apoptosis, 28.89% underwent late apoptosis, and 26.58% underwent necrosis. The apoptosis rates of cells treated with NO are shown in the fourth panel. Overall, 21.20% of the cells

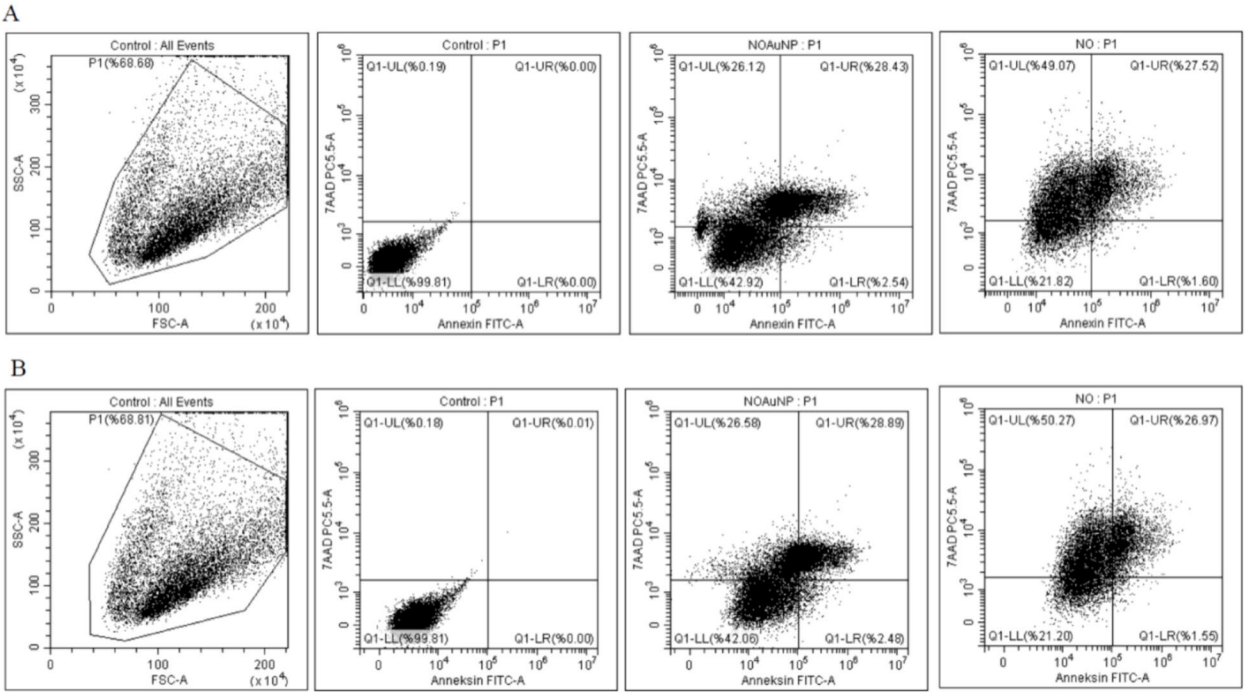

Fig. 10 Annexin FITC/7-AAD staining of A-549 cells at 24 (**A**) and 48 (**B**) hours. Figure 10A and B first show the FS/SS dot blot analysis, specifically their granularity and size. The second, third, and fourth panels show the percentages of apoptotic and necrotic cells in the control, NOAuNP, and NO series, respectively (Fig. 10A and B do not display the FS/SS analysis of the NOAuNP- and NO-treated cells)

in this group were alive, 1.55% were in early apoptosis, 26.97% were in late apoptosis, and 50.27% were necrotic.

As shown in Fig. 10, the percentages of apoptotic A549 cells treated with the IC_{50} doses for 24 and 48 h were very similar. However, the number of cells undergoing apoptosis was high in the NOAuNP group at both time points. In the NO extract group, the number of necrotic cells was high.

Cell cycle analysis by flow cytometry

After staining with propidium iodide (PI), the cell cycle distribution was analyzed in all groups. Flow cytometry was used to examine 10.000 cells from each treatment group. The cell counts in the G0/G1, S, and G2-M stages are expressed as percentages (%). Figure 11 shows the A549 cell cycle flow cytometry results at 24 and 48 h. Figure 11 shows the percentages of cells in various stages of the cell cycle 24 (A) and 48 (B) hours after treatment with the IC_{50} of the NOAuNPs and NO or those receiving no treatment. In general, the percentage of cells in the G0-G1 stage was greater in all groups at 48 h than at 24 h.

Notably, the number of cells in G2-M phase decreased very slightly in the NOAuNP and NO groups after 24 h (Fig. 12A) and 48 h (Fig. 12B). We believe this is because the NOAuNPs and NO arrested the cell

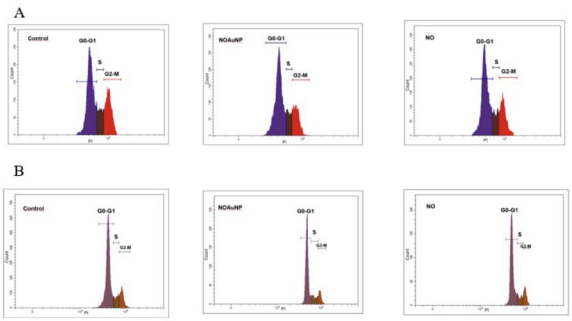

Fig. 11 Cell cycle analysis by flow cytometry after 24 and 48 h in the control, NOAuNP-treated and NO-treated groups: **A** 24 h and **B** 48 h

cycle at G1-G0 or S phase. When we compare the percentage of cells in G1-G0 + S phase to the percentage of cells in G2-M phase (Table 2), we can see that arrest was greatest in the NOAuNP group.

We believe that the above data are the result of the added NOAuNPs and NO extract that arrest the cell cycle in the G1–G0 or S phase. When we compare the number of cells in G1-G0 + S phase to the number of cells in G2-M phase (Table 2), we can see that this arrest was the greatest in the NOAuNP group.

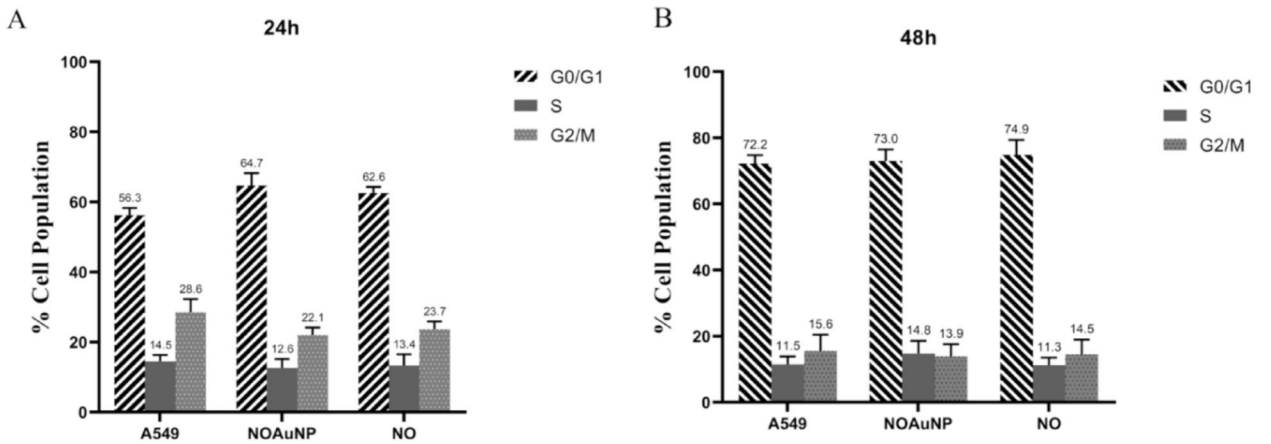

Fig. 12 Cell cycle distribution in the G0/G1, S and G2/M phases at 24 (**A**) and 48 h (**B**) for control, NOAuNP-treated and NO-treated A549 cells (error bars represent the standard deviations of the means from triplicate assays)

Table 2 Comparison of the G0-G1 + S cell/G2-M cell ratio in the control, NOAuNP-treated and NO-treated A549 cells

	Group	Control	NOAuNPs	NO	*P*
24 h	G0-G1 + S (%)/G2-M (%)	2.48	**3.49**	3.20	0.0002
48 h	G0-G1 + S (%)/ G2-M (%)	5.36	**6.31**	5.94	

$p < 0.001$

In silico analysis

The in-silico results for the molecule PEITC, which has been shown to be abundant in plants in the literature, are shown in Table 3. The SwissADME and pkCSM servers were used for ADMET predictions of the highly bioactive substance PEITC. Table 3 displays the findings of the analysis.

The ADMET properties of PEITC were analyzed using SwissADME and pkCSM. PEITC met Lipinski's Ro5 physicochemical criteria, including MA < 500 g/mol, H-donor < 5, H-acceptor < 10, rotatable bonds 10, MLog $P < 5$, and TPSA < 140 Å^2. PEITC also had moderate bioavailability. Table 3 shows that PEITC has high GI absorption. Considering the lipid solubility of the molecule, PEITC has an elevated mLogP, indicating a propensity for lipolysis. Table 3 shows that PEITC can easily cross the BBB. Furthermore, PEITC was neither a cytochrome P450 substrate nor an inhibitor. From the ProTox II web application, PEITC had no toxic effects. Figures 13, 14 and 15 and Table 4 show the docking of the molecule to the enzyme cytochrome P450 and the protein Beta Tubulin.

Discussion

The ability of nanosized materials to exhibit certain physicochemical properties has led to scientific and technological innovations. Nanomaterials can be synthesized with a variety of metals, but silver and gold are among the most extensively researched. Gold nanoparticles are used

Table 3 The physicochemical and absorption, distribution, metabolism, excretion, and toxicity (ADMET) properties of phenethyl isothiocyanate (PEITC)

Molecule	Physicochemical Properties								Drug-likeness (Yes/No)
	Molecular Formula	MW (g/mol)	TPSA (Å^2)	H-Donor	H-Acceptor	Rotatable Bonds	MLOGP (Log $P_{octanol/water}$)	ESOL (Log S)	
PEITC	C9H9NS	163.24	44.45	0	1	3	3.59	−3.24	Yes
ADMET									
Molecule	**GI absorption**	**BBB Perm**	**P-gp substrate (Yes/No)**		**P450 Substrate (Yes/No)**	**P450 Inhibitor (Yes/No)**	**Carcinogenicity/ Ames Toxicity (Yes/No)**	**Bioavailability**	
PEITC	High	Yes	No		No	No	No/No	0.55	

PEITC Phenethyl isothiocyanate, *MW* Molecular weight (g/mol), *TPSA* Topological polar surface area (Å^2), *H-donor* number of H-bond donors, *H-acceptor* number of H-bond acceptors, *MLOGP* Moriguchi octanol–water partition coefficient (Log Poctanol/water), *ESOL* Estimated water solubility (Log S), *GI Absorption* gastrointestinal absorption, *BBB Perm.* blood–brain barrier permeability, *P-gp* P-glycoprotein, *P450* cytochrome P450 enzyme

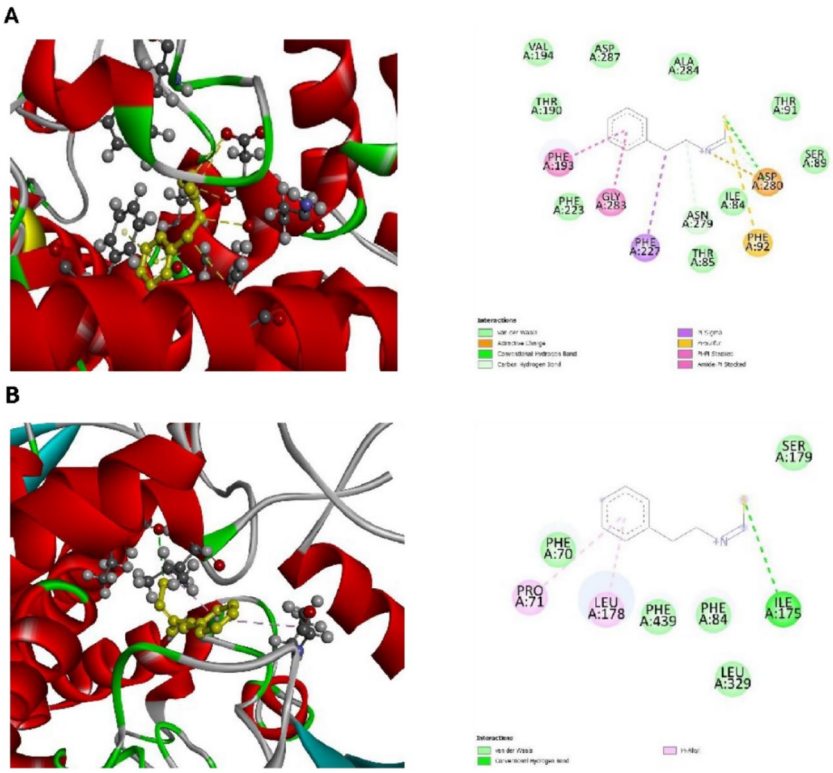

Fig. 13 Interactions between cytochrome P450 enzymes and phenethyl isothiocyanate (PEITC): **A** CYP1A2 and **B** CYP2C9

in a variety of fields beyond sensor production, including medicine, disease treatment, food, biomedicine, and textiles [51]. The emergence of different shapes and sizes of gold nanoparticles, the fact that they can be characterized using various methods, their low toxicity, and their biological compatibility are why they are preferred in current research [52]. In our study, spherical nanoparticles with a size of approximately 56.4 nm were developed, and their shape is consistent with the literature [53, 54].

The primary goal of analyzing he antioxidant activity of extracts and nanoparticles is to determine their ability to reduce damage caused by the free radicals produced via metabolism and various diseases. An increase in the percent inhibition of DPPH free radical scavenging activity indicates that a sample could have a high antioxidant capacity. Other studies with *N. officinale* have shown that the DPPH activity of the plant's methanolic extract is lower than that of the positive control [55]. Amiri [56] evaluated the antioxidant activity of the *N. officinale* methanolic extract and its essential oil using the DPPH test. The extract was found to have greater antioxidant activity than the essential oil but lower antioxidant activity than BHT, which was used as a positive control [56]. In another study, the antioxidant activities of various *N. officinale* organic solvent extracts were investigated using the DPPH test, and the methanolic extract had greater antioxidant activity than the ethyl acetate and hexane extracts did [57]. Our study showed that NO inhibited DPPH by 31.78 ± 1.71%. According to the Ercan and Doğru study [58], the percentage of DPPH free radical inhibition by the *N. officinale* methanol extract (40 µg/ml) was 16.56%. Both of these results reported in the literature [55–58] and our analysis indicate that watercress is a free radical inhibitor and antioxidant that reacts with free radicals. The synthesized AuNPs had an inhibitory effect of 31.62 ± 0.46%, indicating that they do not affect the antioxidant activity of the plant during synthesis; previous ABTS studies have indicated that the percentage of *N. officinale* inhibition increases with the concentration [58, 59]. In a study using aqueous and methanol extracts of *N. officinale*, antioxidant activity was determined using DPPH, ABTS, CUPRAC, and FRAP assays. The results showed that the methanolic extract of *N. officinale* had greater antioxidant activity than the aqueous extract. Our study showed that this plant inhibited ABTS activity by 25.89 ± 1.90%, which is consistent with previous research. At the highest concentration of 200 µg/mL, the NOAuNPs showed 33.81 ± 0.62% inhibition, indicating superior ABTS cation scavenging activity compared to that of the plant. This may be due to the variable physicochemical

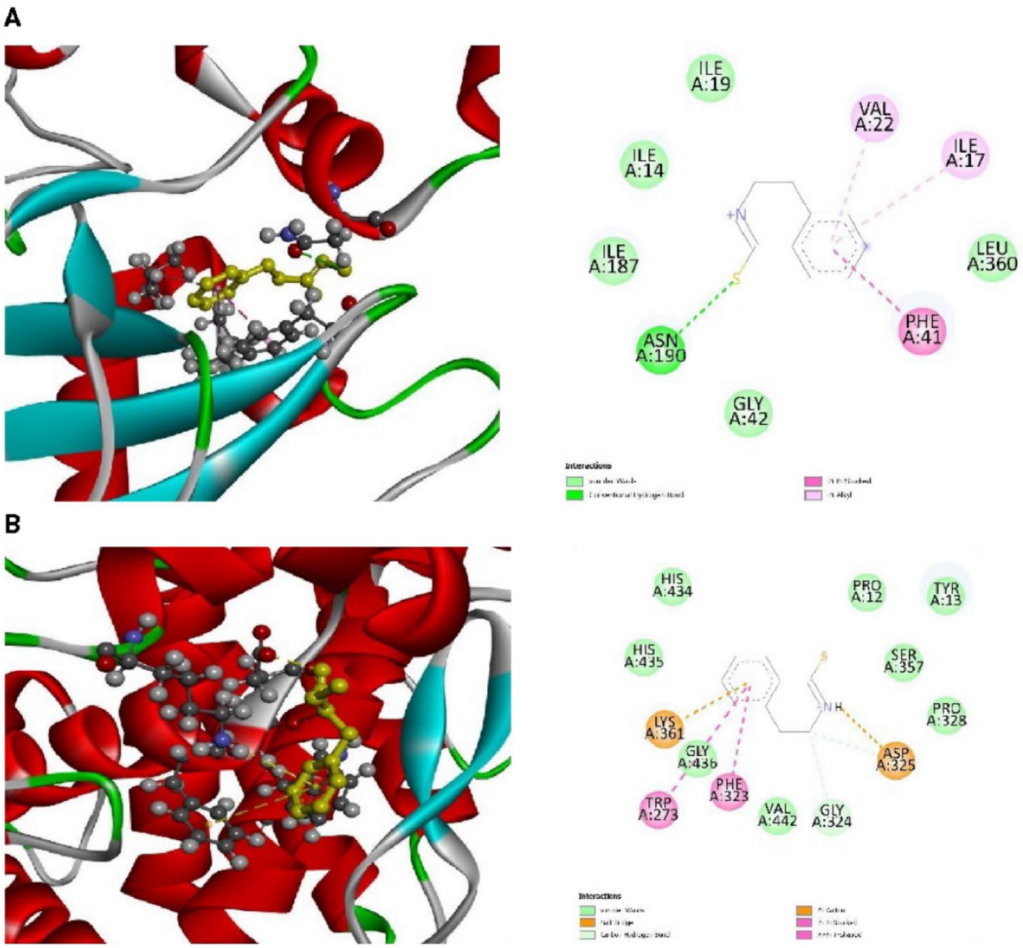

Fig. 14 Interactions between cytochrome P450 enzymes and phenethyl isothiocyanate (PEITC): **A** CYP2C19 and **B** CYP2D6

properties of gold nanoparticles with different shapes and sizes. Previous studies evaluating FRAP and CUPRAC indicate that this plant has iron- and copper-reducing activities [58, 60]. Devendrapandi et al. [61] also reported that gold nanoparticles synthesized from *Aegle marmelos* fruits had anticancer effects on lung cancer cells (A549).

N. officinale, a perennial aquatic plant, has anticancer properties due to its bioactive components such as phenolics and flavonoids. Previous studies have reported that the total phenolic content in watercress is greater in the vegetative period, the total flavonoid content is greater in the productive period, and that plants grown in high-altitude regions also contain more flavonoids and phenolic compounds [62]. In our study, the amount of flavonoids was also greater than that of phenolics. The flavonoid compounds isolated from the leaves and flowers of *N. officinale* have been shown to have anticancer effects on breast cancer cells (T47D) and colon cancer cells (HT-29) [63]. *N. officinale* is well known as an antioxidant-rich source of PEITC. PEITC has been reported to be a chemopreventive agent against prostate, breast, lung, and liver cancer and leukemia [16].

In silico analysis of PEITC from NO revealed that this molecule has high drug-likeness and weakly interacts with the cytochrome P450 enzymes involved in the biotransformation of many drugs. This may reduce the risk of drug–drug interactions that may occur due to the pharmacokinetic properties of drugs and may contribute to great benefits of plant extract-based drug treatment. When examining the drug-likeness of and the ADMET predictions for PEITC, it was observed that this molecule exhibited drug-likeness (Table 3). Predictive models offer advantages, such as throughput and the ability to work with virtual structures, and many promising methods have been published [64]. In the literature, it has been reported that NO contains an acceptable amount of PEITC. Considering both the literature on the efficacy of PEITC and the in-silico data obtained in our study, it is anticipated that due to the lack of interactions between

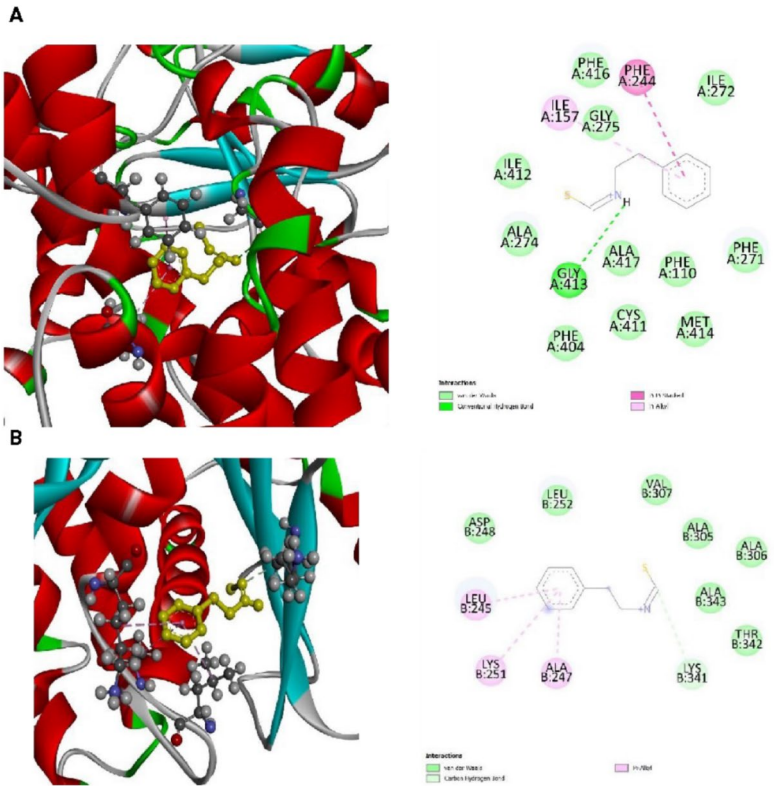

Fig. 15 Interactions between phenethyl isothiocyanate (PEITC) and CYP3A4 and Beta Tubulin: **A** CYP3A4 and **B** Beta Tubulin

Table 4 Ligand–protein docking results

	Receptor/Ligand	ID number	Affinity (kcal/mol)	RMSD l.b	RMSD u.b
Protein Structure	CYP 1A2	PDB 2HI4	-6.8	1.655	2.456
	CYP 3A4	PDB 1TQN	-5.8	2.033	2.211
	CYP 2C19	PDB 4GQS	-5.2	3.651	4.674
	CYP 2C9	PDB 1R9O	-5.0	4.142	4.967
	CYP 2D6	PDB 2F9Q	-4.8	3.872	6.393
	Beta Tubulin	PDB 1SA0	-4.2	3.347	5.335
Ligand	PEITC	PubChem 16,741	-	-	-

PEITC phenethyl isothiocyanate

PEITC bound weakly to the CYP enzymes and Tubulin, as shown in Figs. 13, 14 and 15 and Table 4. According to the SwissADME data, this molecule is not a CYP substrate. The data from both programs corroborated with one another

PEITC and cytochrome P450 enzymes (Figs. 13, 14 and 15), potential drug interactions and toxicity risks could be minimized (Table 4). This suggests significant advantages for PEITC in terms of its safety and tolerability. PEITC demonstrates high solubility in lipids. Such lipophilic characteristics can have significant implications for drug design, bioavailability, and distribution. Considering these findings, drug formulations developed from NO (containing PEITC) are considered promising. Due to their stable structure and lack of cytotoxicity, the anticancer effects of the gold nanoparticles synthesized with *N. officinale* on the lung cancer cell line A549 were evaluated in this study. NOAuNPs reduced A549 cancer cell viability in a dose-dependent manner compared to NO after direct application. NOAuNPs were more effective in this lung cancer cell line than NO at the same doses.

In recent years, natural plant products, such as extracts and nanoparticles made from them, have been

investigated for their antitumor activity [65, 66]. Despite their pharmacological and anticancer properties, the low bioavailability natural compounds is a drawback. To expand the therapeutic applications of these compounds, systems such as liposomes, nanoparticles, and nanoemulsions have been designed and shown to be effective in promoting apoptosis [42]. In multicellular organisms, apoptosis, or programmed cell death, is essential for the development and maintenance of homeostasis during cell growth and is also known as the primary anticancer therapeutic response [67, 68]. Apoptosis signals can be received by cells in a variety of ways. One way is that these signals can enter cells via receptors on the cell surface. The second type of signal is mitochondrial apoptosis, which is triggered by DNA damage, ROS, or molecules that can cross the cell membrane [65]. Caspases and the Bcl-2 family of proteins play important roles in the regulation of apoptosis. The release of cytochrome C into the cytoplasm initiates the mitochondrial apoptosis pathway. This causes the activation of effector caspases. Phosphatidylserine in the inner layer of the cell membrane migrates to the outer layer of the membrane during the early stages of apoptosis. The cytoskeleton and nuclear lamina undergo structural changes and DNA fragmentation occurs. During late apoptosis, DNA fragmentation begins to occur [66]. In this study, A549 cells were treated with NOAuNPs or NO for 24 or 48 h, the IC_{50} values were determined, and flow cytometry (Annexin-V/7-AAD) was used to quantify the ratios of apoptotic and necrotic cells. As shown in Figs. 11 and 12, the cells treated with NOAuNPs and NO had significantly greater apoptosis rates than the control cells. Furthermore, NOAuNPs increased the proportions of cells in both early and late apoptosis.

Necrosis, another type of cell death in which the cell integrity is disrupted, results in pathological death and inflammation [53]. We found that the number of necrotic cells was greater in the NO-treated group. Thus, the nanoformulated NO compounds were shown to have greater therapeutic and anticancer effects. Based on our findings, NOAuNPs are thought to contribute to the induction of apoptosis and a reduction in necrosis.

Aldravan et al. investigated the apoptotic effects of NO and NO nanoparticles in A549 cells and discovered that the degree of apoptosis induced by NO-loaded PLGA/PEG NPs was high, with increases in the rates of early and late apoptotic cell rates compared to those of the control, similar to our results. We believe that the difference in necrosis rates observed in our study is due to the type of nanoparticle used. Furthermore, in the present study, the expression levels of the mitochondrial apoptotic proteins p53, Bax, and Caspase 3 increased, while the expression levels of the antiapoptotic proteins Bcl-2 and Cyclin D1 decreased [68, 69]. In publications showing the apoptotic effect of NO on cancer cells, there is evidence that isothiocyanates and their metabolites increase the sensitivity of cancer cells to apoptosis. Western blot analysis revealed that these proteins induce the cleavage of apoptotic caspases 3, 7, 8, and 9 and PARP and cause Bcl-2 downregulation and Bax overexpression in PC-3 human prostate cancer cells and bladder cancer cells [70, 71]. Munday et al. [72] added an extract of broccoli (from the family Cruciferae) to the diets of rats with bladder cancer and investigated its effects on tumor tissue. They detected significant reductions in the incidence, multiplicity, size and progression of bladder cancer. In addition to members of the Cruciferae family, glucosinolates also exert anticancer effects by inducing proteins related to apoptosis [73, 74].

Flow cytometry revealed that NOAuNP treatment of A549 cells resulted in cell cycle arrest in the G0/G1 phase after 24 and 48 h. The percentage of cells retained in this phase was greater at 48 h (Fig. 12). In addition, when we compared the percentage of cells in the G2/M phase, which is the basic phase of cell division, to those in the other interphase phases, we discovered that the cells in the NO and NOAuNP groups were arrested before G2/M. The NOAuNP group had the greatest arrest, and the differences were statistically significant ($p < 0.05$). In Huh7 hepatoma cells, atractylodin, an herbal product, caused a gradual increase in the number of cells in G1 phase and a gradual decrease in the number of cells in G2 phase [75]. Another cell cycle study with A549 cells using different NONPs revealed that the cells remained in S phase. While G0/G1 arrest was most notable in our study, the ratios of cells in the G0/G1 and S phases to those in G2/ cells increased significantly, particularly in the NOAuNP group (Table 2). Cell cycle arrest in G1, S, and/or G2/M phases is caused by DNA damage [76]. The apoptotic effects of NO and the NOAuNPs are linked to changes in cell cycle progression, particularly G0/G1 phase arrest. According to these findings, inhibiting cell cycle progression is likely one of the antitumor molecular mechanisms of NO and the NOAuNPs.

Conclusion

The NO and NOAuNPs were used to evaluate the antitumor effect of NO on lung cancer cells. The AuNPs more effectively reduced cell viability than NO. Both the extract and the AuNPs induced cell apoptosis while keeping the cells in G0/G1 phase. The NOAuNPs strongly induce both apoptosis and cell cycle inhibition. We believe this is due to the AuNPs mediating NO uptake by cancer cells.

In our study, we successfully synthesized AuNPs from NO. In addition, we confirmed that the green-synthesized nanoparticles had a greater toxicity to A 549 lung cancer cells than control treatment. This result indicates that the AuNPs prepared with the NO can be used as anticancer agents for lung cancer treatment. However, in vivo studies should be performed to fully confirm our results and to elucidate the underlying mechanisms of action.

Abbreviations

ABTS	2,2′-Azino-bis(3-ethylbenzothiazoline-6-sulfonic acid)
ADMET	Drug likeness and absorption, distribution, metabolism, excretion, and toxicity
AuNPs	Gold nanoparticles
BHT	Butylated hydroxytoluene
CUPRAC	Copper ion reducing antioxidant capacity
CYP 450	Cytochrome P450
DMEM	Dulbecco's modified Eagle's medium
DMSO	Dimethyl sulfoxide
DPPH	1,1-Diphenyl-2-picrylhydrazyl
EDS	Energy dispersive X-ray spectrometry
FBS	Fetal bovine serum
FRAP	Ferrous ion reducing antioxidant capacity
FT-IR	Fourier transform infrared spectroscopy
GA	Gallic acid
HIV	Human immunodeficiency virus
IC_{50}	50% Suppressive concentration
ITC	Isothiocyanate
MAP	Multiple analysis platform
MTT	3-(4,5-Dimethylthiazol-2-il)-2,5-diphenyltetrazolium bromide
NO	*Nasturtium officinale* (L.) extract
N. officinale	*Nasturtium officinale* (L.)
NOAuNPs	*Nasturtium officinale* Gold nanoparticles
NPs	Nanoparticles
PEITC	Phenethyl isothiocyanate
PDB	Protein Data Bank
SEM	Scanning electron microscopy
SMILES	Simplified molecular input line entry system
SPR	Surface plasmon resonance
TEM	Transmission electron microscopy
UV–Vis	Ultraviolet–visible spectrophotometry
WHO	World Health Organization

Acknowledgements
All authors acknowledge the Çanakkale Onsekiz Mart University Scientific Research Projects Coordination Unit.

Disclosure statement
No potential conflict of interest was reported by the author(s).

Authors' contributions
O.T.Y.: conceptualization, methodology, data curation, writing—original draft, writing—review and editing, project administration; N.D.: methodology, writing—original draft, data analysis, investigation, visualization; F.C.: methodology, writing—original draft, software, data analysis; T.K.A.: methodology, formal analysis, validation, visualization; M.P.: methodology, formal analysis, validation, visualization. All authors read and approved the final manuscript.

Funding
This study was organized with project data numbered TSA-2022–3921 supported by Çanakkale Onsekiz Mart University Scientific Research Projects Coordination Unit.

Availability of data and materials
Data is provided within the manuscript.

Declarations

Ethics approval and consent to participate
Not applicable.

Consent for publication
Not applicable.

Competing interests
The authors declare no competing interests.

Author details
[1]Faculty of Medicine, Çanakkale Onsekiz Mart University, Çanakkale, Turkey. [2]Department of Biology, Çanakkale Onsekiz Mart University Faculty of Science, Çanakkale, Turkey. [3]Department of Pharmacy Services, Çanakkale Onsekiz Mart University, Vocational School of Health Services, Çanakkale, Turkey. [4]Faculty of Medicine, Medical Biology Department, İzmir Katip Çelebi University, İzmir, Turkey. [5]İzmir Katip Çelebi University, Vocational School of Health Services, İzmir, Turkey.

Received: 21 March 2024 Accepted: 6 September 2024
Published online: 01 October 2024

References

1. Jamshidi-Kia F, Lorigooini Z, Amini-Khoei H. Medicinal plants: Past history and future perspective. J Herbmed Pharmacol. 2017;7(1):1–7. https://doi.org/10.15171/jhp.2018.01.
2. Awuchi CG. Medicinal plants: the medical, food, and nutritional biochemistry and uses. International Journal of Advanced Academic Research. 2019;5(11):220–41.
3. Wangchuk P. Therapeutic applications of natural products in herbal medicines, biodiscovery programs, and biomedicine. Journal of Biologically Active Products from Nature. 2018;8(1):1–20. https://doi.org/10.1080/22311866.2018.1426495.
4. Musthaba M, Baboota S, Athar TMD, Thajudeen KY, Ahmed S, Ali J. Patented herbal formulations and their therapeutic applications. Recent Pat Drug Delivery Formulation. 2020;4(3):231–44. https://doi.org/10.2174/187221110793237538.
5. Lam TK, Gallicchio L, Lindsley K, Shiels M, Hammond E, Tao X, Chen L, Robinson KA, Caulfield LE, Herman JG, Guallar E, Alberg AJ. Cruciferous vegetable consumption and lung cancer risk: A systematic review. Cancer Epidemiol Biomarkers Prev. 2009;18:184–95. https://doi.org/10.1158/1055-9965.EPI-08-0710.
6. Ambrosone CB, Mc Cann SE, Freudenheim JL, Marshall JR, Zhang Y, Shields PG. Breast cancer risk in premenopausal women is inversely associated with consumption of broccoli, a source of isothiocyanates, but is not modified by GST genotype. J Nutr. 2004;134(5):1134–8. https://doi.org/10.1093/jn/134.5.1134.
7. Steinbrecher A, Nimptsch K, Hüsing A, Rohrmann S, Linseisen J. Dietary glucosinolate intake and risk of prostate cancer in the EPIC-Heidelberg cohort study. Int J Cancer. 2009;125(9):2179–86. https://doi.org/10.1002/ijc.24555.
8. Hansson LE, Nyren O, Bergstro MR. Diet and risk of gastric cancer: A population-based case-control study in Sweden. Int J Cancer. 1993;55:181–9.
9. Epplein M, Wilkens LR, Tiirikainen M, Dyba M, Chung FL, Goodman MT, Murphy SP, Henderson BE, Kolonel LN, Le Marchand L. Urinary isothiocyanates; glutathione s-transferase M1, T1, and P1 polymorphisms; and risk of colorectal cancer: The multiethnic cohort study. Cancer Epidemiol Biomarkers Prev. 2009;18(1):314–20. https://doi.org/10.1158/1055-9965.EPI-08-0627.
10. Verhoeven DT, Verhagen H, Goldbohm RA, Van Den Brandt PA, Van Poppel GA. Review of mechanisms underlying anticarcinogenicity by brassica vegetables. Chem Biol Interact. 1997;103:79–129. https://doi.org/10.1016/S0009-2797(96)03745-3.
11. Talalay P, Fahey JW. Phytochemicals from cruciferous plants protect against cancer by modulating carcinogen metabolism. J Nutr. 2001;131(11):3027–33. https://doi.org/10.1093/jn/131.11.3027S.

12. Conaway CC, Jiao D, Kohr T, Liebes L, Chung FL. Disposition and pharmacokinetics of phenethyl isothiocyanate and 6-phenylhexyl isothiocyanate in F344 rats. Drug Metab Dispos. 1999;27(1):13–20.
13. Salehi B, Quispe C, Butnariu M, Sarac I, Marmouzi I, Kamle M, Tripathi V, Kumar P, Bouyahya A, Capanoglu E, Ceylan FD, Singh L, Bhatt ID, Sawicka B, Krochmal-Marczak B, Skiba D, El Jemli M, El Jemli Y, Coy-Barrera E, Sharifi-Rad J, Kamiloglu S, Cádiz-Gurrea ML, Segura-Carretero A, Kumar M, Martorell M, Martorell M. Phytotherapy and food applications from Brassica genus. Phytother Res. 2021;35(7):3590–609. https://doi.org/10.1002/ptr.7048.
14. Kyriakou S, Michailidou K, Amery T, Stewart K, Winyard PG, Trafalis DT, Franco R, Pappa A, Panayiotidis MI. Polyphenolics, glucosinolates and isothiocyanates profiling of aerial parts of Nasturtium officinale (Watercress). Front Plant Sci. 2022;13: 998755. https://doi.org/10.3389/fpls.2022.998755.
15. Silveira AC, Araneda C, Hinojosa A, Escalona VH. Effect of non-conventional modified atmosphere packaging on fresh cut watercress (Nasturtium officinale R. Br.) quality. Postharvest Biol Technol. 2014;92:114–20. https://doi.org/10.1016/j.postharvbio.2013.12.012.
16. Kyriakou S, Potamiti L, Demosthenous N, Amery T, Stewart K, Winyard PG, Panayiotidis MI. A naturally derived watercress flower-based phenethyl isothiocyanate-enriched extract induces the activation of intrinsic apoptosis via subcellular ultrastructural and Ca^{2+} efflux alterations in an in vitro model of human malignant melanoma. Nutrients. 2023;15(18):4044. https://doi.org/10.3390/nu15184044.
17. Wang Q, Bao Y. Nanodelivery of natural isothiocyanates as a cancer therapeutic. Free Radical Biol Med. 2021;167:125–40. https://doi.org/10.1016/j.freeradbiomed.2021.02.044.
18. Thatyana M, Dube NP, Kemboi D, Manicum A-LE, Mokgalaka-Fleischmann NS, Tembu JV. Advances in Phytonanotechnology: A plant-mediated green synthesis of metal nanoparticles using phyllanthus plant extracts and their antimicrobial and anticancer applications. Nanomaterials. 2023;13(19):2616. https://doi.org/10.3390/nano13192616.
19. Hammami I, Alabdallah NM. Gold nanoparticles: Synthesis properties and applications. J King Saud Univ Sci. 2021;33(7):101560. 1-10. https://doi.org/10.1016/j.jksus.2021.101560.
20. Singh N, Manshian B, Jenkins GJS, Griffiths SM, Williams PM, Maffeis TG, Wright CJ, Doak SH. NanoGenotoxicology: The DNA damaging potential of engineered nanomaterials. Biomaterials. 2009;30:3891–914. https://doi.org/10.1016/j.biomaterials.2009.04.009.
21. Hassanisaadi M, Bonjar GHS, Rahdar A, Pandey S, Hosseinipour A, Abdolshahi R. Environmentally Safe Biosynthesis of Gold Nanoparticles Using Plant Water Extracts. Nanomaterials. 2021;11(8):2033. https://doi.org/10.3390/nano11082033.
22. Kyzioł A, Łukasiewicz S, Sebastian V, Kuśtrowski P, Kozieł M, Majda D, Cierniak A. (Towards plant-mediated chemistry–Au nanoparticles obtained using aqueous extract of *Rosa damascena* and their biological activity in vitro. J Inorg Biochem. 2021;214(11300):1–14. https://doi.org/10.1016/j.jinorgbio.2020.111300.
23. Demirtas H, Türk CS. Altın Nanopartiküller ve kanserde kullanımları. J Faculty Pharm Ankara Univ. 2021;45(1):70–95. https://doi.org/10.33483/jfpau.773430.
24. Beik J, Khateri M, Khosravi Z, Kamrava SK, Kooranifar S, Habib Ghaznavi H, Shakeri-Zadeh A. Gold Nanoparticles in Combinatorial Cancer Therapy Strategies. Coord Chem Rev. 2019;387:299–324. https://doi.org/10.1016/j.ccr.2019.02.025.
25. Skinner AV, Han S, Balasubramian R. Rapid selective colorimetric sensing of polyphosphates by ionic resorcinarene cavitand interdigitated gold nanoparticles. Sens Actuators, B Chem. 2017;247:706–12. https://doi.org/10.1016/j.snb.2017.03.097.
26. Jayaseelan C, Ramkumar R, Rahuma AA, Perumal P. Green Synthesis of Gold Nanoparticles Using Seed Aqueous Extract of *Abelmoschus esculentus* and its Antifungal Activity. Ind Crops Prod. 2013;45:423–9. https://doi.org/10.1016/j.indcrop.2012.12.019.
27. Chandran SP, Chaudhary M, Pasricha R, Ahmad A, Sastry M. Synthesis of gold nanotriangles and silver nanoparticles using *Aloe vera* plant extract. Biotechnol Prog. 2006;22(2):577–83. https://doi.org/10.1021/bp0501423.
28. Aswathy AS, Philip D. Green synthesis of gold nanoparticles using *Trigonella foenum-graecum* and its size-dependent catalytic activity. Molecular and Biomolecular Spectroscopy. 2012;97:1–5. https://doi.org/10.1016/j.saa.2012.05.083.
29. Kaviya S, Santhanalakshmi J, Viswanathan B, Muthumary J, Srinivasan K. Biosynthesis of silver nanoparticles using *Citrus sinensis* peel extract and its antibacterial activity. Molecular and Biomolecular Spectroscopy. 2011;79(3):594–8. https://doi.org/10.1016/j.saa.2011.03.040.
30. Smitha SL, Philip D, Gopchandran KG. Green synthesis of gold nanoparticles using *Cinnamomum zeylanicum* leaf broth. Spectrochim Acta Part A Mol Biomol Spectrosc. 2009;74(3):735–9. https://doi.org/10.1016/j.saa.2009.08.007.
31. Gardea-Torresdey JL, Parsons JG, Gomez E, Peralta-Videa J, Troiani HE, Santiago P, Yacaman MJ. Formation and Growth of Au Nanoparticles inside Live Alfalfa Plants. Nano Lett. 2002;2(4):397–401. https://doi.org/10.1021/nl015673+.
32. Ankamwar B, Chaudhary M, Sastry M. Gold nanotriangles biologically synthesized using tamarind leaf extract and potential application in vapor sensing. Synth React Inorg, Met-Org, Nano-Met Chem. 2005;35(1):19–26. https://doi.org/10.1081/SIM-200047527.
33. Dubey SP, Lahtinen M, Sillanpää M. Green synthesis and characterizations of silver and gold nanoparticles using leaf extract of *Rosa rugosa*. Colloids Surf, A. 2010;364:34–41. https://doi.org/10.1016/j.colsurfa.2010.04.023.
34. Mobaraki F, Momeni M, Barghbani M, Far BF, Hosseinian S, Hosseini MS. Extract-mediated biosynthesis and characterization of gold nanoparticles: Exploring their protective effect against cyclophosphamide-induced oxidative stress in rat testis. Journal of Drug Delivery Science and Technology. 2022;71: 103306. https://doi.org/10.1016/j.jddst.2022.103306.
35. Canbolat F, Demir N, Yayıntas OT, Pehlivan M, Eldem A, Ayna TK, Senel M. Chitosan nanoparticles loaded with quercetin and valproic acid: A novel approach for enhancing antioxidant activity against oxidative stress in the SH-SY5Y human neuroblastoma cell line. Biomedicines. 2024;12(2):287. https://doi.org/10.3390/biomedicines12020287.
36. Matejić JS, Džamić AM, Mihajilov-Krstev TM, Ranđelović VN, Krivošej ZĐ, Marin PD. Total phenolic and flavonoid content, antioxidant, and antimicrobial activity of extracts from *Tordylium maximum*. Journal of Applied Pharmaceutical Science. 2013;3(1):55–9. https://doi.org/10.7324/JAPS.2013.30110.
37. Slinkard K, Singleton VL. Total phenol Analysis: Automation and comparison with manual methods. Am J Enol Vitic. 1977;28(1):49–55. https://doi.org/10.5344/ajev.1977.28.1.49.
38. Blois MS. Antioxidant determinations by the use of a free radical. Nature. 1958;181:1199–200. https://doi.org/10.1038/1811199a0.
39. Re R, Pellegrini N, Proteggente A, Pannala A, Yang M, Rice-Evans C. Antioxidant activity applying an improved ABTS radical cation decolorization assay. Free Radic Biol Med. 1999;26(9–10):1231–7.
40. Benzie IF, Strain JJ. The ferric reducing ability of plasma (FRAP) as a measure of "antioxidant power." The FRAP assay Analytical Biochemistry. 1996;239(1):70–6. https://doi.org/10.1006/abio.1996.0292.
41. Apak R, Güçlü K, Özyürek M, Karademir SEN, Altun M. Total antioxidant capacity assay of human serum using copper (II)-neocuproine as chromogenic oxidant: The CUPRAC method. Free Radical Res. 2005;39(9):949–61. https://doi.org/10.1080/10715760500210145.
42. Sun B, Hu N, Han L, Pi Y, Gao Y, Chen K. Anticancer activity of green synthesised gold nanoparticles from *Marsdenia tenacissima* inhibits A549 cell proliferation through the apoptotic pathway. Artificial cells, nanomedicine, and biotechnology. 2019;47(1):4012–9. https://doi.org/10.1080/21691401.2019.1575844.
43. Tian Y, Li P, Xiao Z, Zhou J, Xue X, Jiang N, Peng C, Wu L, Tian H, Popper H, Poh ME, Marcucci F, Zhang C, Zhao X. Triptolide inhibits epithelial-mesenchymal transition phenotype through the p70S6k/GSK3/β-catenin signaling pathway in taxol-resistant human lung adenocarcinoma. Transl lung Cancer Res. 2021;10(2):1007–19. https://doi.org/10.21037/tlcr-21-145.
44. Lipinski CA, Lombardo F, Dominy BW, Feeney PJ. Experimental and computational approaches to estimate solubility and permeability in drug discovery and development settings. Adv Drug Deliv Rev. 1997;23:3–25. https://doi.org/10.1016/S0169-409X(96)00423-1.
45. Ghose AK, Viswanadhan VN, Wendoloski JJ. A knowledge-based approach in designing combinatorial or medicinal chemistry libraries for drug discovery. A qualitative and quantitative characterization of known drug databases. J Comb Chem. 1999;1:55–68. https://doi.org/10.1021/cc9800071.

46. Lipinski CA. Drug-like properties and the causes of poor solubility and poor permeability. J Pharmacol Toxicol Methods. 2000;44:235–49. https://doi.org/10.1016/S1056-8719(00)00107-6.
47. Daina A, Michielin O, Zoete V. SwissADME: A free web tool to evaluate pharmacokinetics, drug-likeness and medicinal chemistry friendliness of small molecules. Sci Rep. 2017;7:42717. https://doi.org/10.1038/srep42717.
48. Pires DE, Blundell TL, Ascher DB. pkCSM: Predicting small-molecule pharmacokinetic and toxicity properties using graph-based signatures. J Med Chem. 2004;58:4066–72. https://doi.org/10.1021/acs.jmedchem.5b00104.
49. Azzam KA KA. SwissADME & pkCSM webservers predictors. An integrated online platform for accurate and comprehensive predictions for in silico ADME/T properties of artemisinin and its derivatives. Complex Use Miner Resour. 2023;325:14–21. https://doi.org/10.31643/2023/6445.13.
50. Lagarde N, Zagury JF, Montes M. Importance of the pharmacological profile of the bound ligand in enrichment on nuclear receptors: toward the use of experimentally validated decoy ligands. J Chem Inf Model. 2014;54(10):2915–44.
51. Huang M, Xiong E, Wang Y, Hu M, Yue H, Tian T, Zhu D, Liu H, Zhou X. Fast microwave heating-based one-step synthesis of DNA and RNA modified gold nanoparticles. Nat Commun. 2022;13(1):968. https://doi.org/10.1038/s41467-022-28627-8.
52. Alsikhan M, Al-Fakeh M, Alminderej F, El-Sayed WA. Review: Gold nanoparticles in biomedical anti-cancer applications. Journal of Qassim University for Science. 2022;1(1):90–128.
53. Pourhassan-Moghaddam M, Zarghami N, Mohsenifar A, Rahmati-Yamchi M, Gholizadeh D, Akbarzadeh A, De la Guardia M, Nejati-Koshki K. Watercress-based gold nanoparticles: biosynthesis, mechanism of formation and study of their biocompatibility in vitro. Micro & Nano Letters. 2014;9(5):345–50. https://doi.org/10.1049/mnl.2014.0063.
54. Ali S, Iqbal M, Naseer A, Yaseen M, Bibi I, Nazir A, Khan MI, Tamam N, Alwasai N, Rizwan M, Abbas M. State of the art of gold (Au) nanoparticles synthesis via green routes and applications: A review. Environmental Nanotechnology, Monitoring & Management. 2021;16: 100511. https://doi.org/10.1016/j.enmm.2021.100511.
55. Al-Snafi AE. A review on *Nasturtium officinale*: A potential medicinal plant. IOSR Journal of Pharmacy. 2020;10(9):33–43.
56. Amiri H. Volatile constituents and antioxidant activity of flowers, stems and leaves of *Nasturtium officinale* R. Br Natural Product Research. 2012;26(2):109–15. https://doi.org/10.1080/14786419.2010.534998.
57. Haro G, Iksen I, Rumanti RM, Marbun N, Sari RP, Gultom RPJ. Evaluation of antioxidant activity and minerals value from watercress (*Nasturtium officinale* R. Br.). Rasayan J Chem. 2018;11(1):232–7. https://doi.org/10.7324/RJC.2018.1112011.
58. Ercan L, Doğru M. The Investigation on Antioxidant Activities of Nasturtium Officinale Extracts and Its Mineral Content. Dicle Üniversitesi Fen Bilimleri Enstitüsü Dergisi. 2021;10(2):197–208.
59. Bahramikia S, Yazdanparast R. Antioxidant efficacy of *Nasturtium officinale* extracts using various in vitro assay systems. J Acupunct Meridian Stud. 2010;3(4):283–90. https://doi.org/10.1016/S2005-2901(10)60049-0.
60. Yazdanparast R, Bahramikia S, Ardestani A. *Nasturtium officinale* reduces oxidative stress and enhances antioxidant capacity in hypercholesterolaemic rats. Chem Biol Interact. 2008;172(3):176–84. https://doi.org/10.1016/j.cbi.2008.01.006.
61. Devendrapandi G, Sahay MI, Padmanaban D, Panneerselvam A, Palraj R, Thanikasalam R, Kuppan S, Sadaiyandi V, Balu R, Rajendiran N. Biogenic synthesis of gold nanoparticles using bael fruit juice and its efficacy against human A-549 lung cancer cell line. Inorg Chem Commun. 2023;151: 110636. https://doi.org/10.1016/j.inoche.2023.110636.
62. Mazandarani M M, Momeji A, A, Zarghami MP MP. . Evaluation of phytochemical and antioxidant activities from different parts of *Nasturtium officinale* R. Br. in Mazandaran. Iranian J Plant Physiol. 2013;3(2):659–64. https://sid.ir/paper/626386/en.
63. Sefidkon F, Torabi B, Naderi M. Comparison of anticancer effects of nanocapsules of *Nasturtium officinalis* (L.) R. Br. extract with methanolic extract andits fractions. Iranian J Med Aromatic Plants. 2013;29(1):35–50. https://doi.org/10.22092/ijmapr.2013.2876.
64. Canbolat F, Kantarci-Carsibasi N, Isik S, Shamshir SRM, Girgin M. Identification of the Candidate mGlu2 Allosteric Modulator THRX-195518 through In Silico Method and Evaluation of Its Neuroprotective Potential against Glutamate-Induced Neurotoxicity in SH-SY5Y Cell Line. Curr Issues Mol Biol. 2024;46(1):788–807. https://doi.org/10.3390/cimb46010051.
65. Elmore S. Apoptosis: a review of programmed cell death. Toxicol Pathol. 2007;35(4):495–516. https://doi.org/10.1080/01926230701320337.
66. D'Arcy MS. Cell death: a review of the major forms of apoptosis, necrosis and autophagy. Cell Biol Int. 2019;43(6):582–92. https://doi.org/10.1002/cbin.11137.
67. Jie M, Kenan H, Hua T, Xinyu D, Chen Q, Xiong Q, Zhifei X. Phloretin induces apoptosis of non-small cell lung carcinoma A549 cells via JNK1/2 and p38 MAPK pathways. Oncol Rep. 2015;34(6):2871–9. https://doi.org/10.3892/or.2015.4325.
68. Adlravan E, Jalilzadeh-Razin S, Nejati K, Karimi MA, Mousazadeh H, Abbasi A, Dadashpour M. Potential activity of free and PLGA/PEG nano encapsulated *Nasturtium officinale* extract in inducing cytotoxicity and apoptosis in human lung carcinoma A549 cells. Journal of Drug Delivery Science and Technology. 2020;61: 102256. https://doi.org/10.1016/j.jddst.2020.102256.
69. Taghavinia F, Teymouri F, Farokhrouz F, Bagherabad EH, Farjami S, Karimi E, Oskoueian E, Le HH, Shakeri M. Nanoliposome-loaded phenolics from *Nasturtium officinale* improves health parameters in a colorectal cancer mouse model. Animals. 2022;12(24):3492. https://doi.org/10.3390/ani12243492.
70. Singh A. Sulforaphane induces caspase-mediated apoptosis in cultured pc-3 human prostate cancer cells and retards growth of pc-3 xenografts in vivo. Carcinogenesis. 2004;25(1):83–90. https://doi.org/10.1093/carcin/bgg178.
71. Abbaoui B, Riedl KM, Ralston RA, Thomas-Ahner JM, Schwartz SJ, Clinton SK, Mortazavi A. Inhibition of bladder cancer by broccoli isothiocyanates sulforaphane and erucin: characterization, metabolism, and interconversion. Mol Nutr Food Res. 2012;56(11):1675–87. https://doi.org/10.1002/mnfr.201200276.
72. Munday R, Mhawech-Fauceglia P, Munday CM, Paonessa JD, Tang L, Munday JS, Lister C, Wilson P, Fahey WJ, Daren W, Zhang Y. Inhibition of urinary bladder carcinogenesis by broccoli sprouts. Can Res. 2008;68(5):1593–600. https://doi.org/10.1158/0008-5472.CAN-07-5009.
73. Cirmi S, Ferlazzo N, Gugliandolo A, Musumeci L, Mazzon E, Bramanti A, Navarra M. Moringin from *Moringa oleifera* seeds inhibits growth, arrests cell-cycle, and induces apoptosis of sh-sy5y human neuroblastoma cells through the modulation of nf-κb and apoptotic related factors. Int J Mol Sci. 2019;20(8):1930. https://doi.org/10.3390/ijms20081930.
74. Bassan P, Bhushan S, Kaur T, Arora R, Vig AP AP. Extraction, profiling and bioactivity analysis of volatile glucosinolates present in oil extract of *Brassica juncea* var. *raya*. Physiol Mol Biol Plants. 2018;24(3):399–409. https://doi.org/10.1007/s12298-018-0509-4.
75. He Y, Fang D, Liang T, Pang H, Nong Y, Yang Z, Lu C, Han X, Zhao S, Mo S, Meng Y, Han C, Peng T. Atractylodin may induce ferroptosis of human hepatocellular carcinoma cells. Ann Transl Med. 2021;9:1535. https://doi.org/10.21037/atm-21-4386.
76. Murray JM, Carr AM. Integrating DNA damage repair with the cell cycle. Curr Opin Cell Biol. 2018;52:120–5. https://doi.org/10.1016/j.ceb.2018.03.006.

Publisher's Note